MASTERARBEIT/MASTER'S THESIS

Titel der Masterarbeit / Title of the Master's Thesis

„SEISMIC HAZARD OF THE SLOVAK TERRITORY CHARACTERIZED BY THE MACROSEISMIC INTENSITY"

verfasst von / submitted by

Martin Šugár, Bc.

angestrebter akademischer Grad / in partial fulfilment of the requirements for the degree of

Master of Science (MSc)

Wien, 2018 / Vienna, 2018

Studienkennzahl lt. Studienblatt / degree programme code as it appears on the student record sheet:	A 066 680
Studienrichtung lt. Studienblatt / degree programme as it appears on the student record sheet:	Joint-Masterstudium Physics of the Earth (Geophysics)
Betreut von / Supervisor:	RNDr. Róbert Kysel, PhD.

I declare that I worked on this thesis on my own, with help from the supervisor and using only sources mentioned in References section.

....
Martin Šugár

Acknowledgement
I would like to thank to my supervisor, RNDr. Róbert Kysel, PhD. for friendly approach and very helpful supervision, to prof. RNDr. Peter Moczo, DrSc. for bringing my attention to the wonderful world of seismology and to doc. Mgr. Jozef Kristek, PhD., Mgr. Martin Gális, PhD. and Mgr. Zuzana Chovanová for frequent and very helpful consultations.

CONTENTS

Introduction

Seismic hazard analysis is an important and necessary part of design of building, e.g. design of important structures such as nuclear power plants or water dams, not only in countries with high seismic hazard, but also in countries with medium seismic hazard like Slovakia.

The master´s thesis deals with seismic hazard analysis of the Slovak territory in terms of macroseismic intensity. Macroseismic intensity is an easily understandable characteristic of ground motion. The advantage of macroseismic intensity is that it requires no instrumentation and measurements of earthquake size are done only by observations.

The first chapter of the thesis is theoretical and deals with definitions of basic term used in seismic hazard analysis. It describes various ground motion characteristics with emphasis on macroseismic intensity and intensity scales. It describes two basic approaches to seismic hazard analysis and describes the mathematical aspects of probabilistic approach to seismic hazard analysis.

The second chapter sums up previous seismic hazard analyses of the Slovak territory in terms of macroseismic intensity.

The third chapter lists the objectives of the presented thesis.

The fourth chapter deals with the compilation of earthquake catalogue for the Slovak territory and small parts of neighbouring countries and its analysis - homogenization, determination of foreshocks, mainshocks and aftershocks (declustering) and determination of time completeness of the catalogue.

The fifth chapter sums up available intensity prediction equations that can be considered for Slovak territory and compares its characteristics.

The sixth chapter of the thesis describes two applied seismotectonic models – SESAME and SK2011.

The seventh chapter deals with characterization of seismic source zones for SK2011 model by input parameters necessary for hazard computation.

The eighth chapter presents seismic hazard maps computed for various input parameters, compares the changes in results caused by the changes in input parameters and compares the results of our new analyses with the previous ones.

1 Seismic hazard analysis

1.1 Basic definitions of terms used in seismic hazard analysis

Although many authors deal with the issues of seismic hazard analysis, they sometimes vary in the basic definitions of terms they use. That´s why it is important to define basic terms used later in the presented thesis.

The following definitions of terms used in seismic hazard analysis are according to McGuire (2004) and Reiter (1990).

Earthquake is defined as the entire phenomenon of rupture on the fault which releases strain stored in the Earth´s crust and propagating energy from the source in the form of (seismic) waves in all directions.

Earthquake damage is defined as a destructive physical effect of the earthquake on a natural or artificial structure e.g effects of the seismic shaking on the buildings.

Seismic hazard is defined as a potential of physical phenomena associated with the earthquakes (for example ground motion or tsunami waves) to cause damages on nature and buildings and/or losses of lives on the given area of the interest.

Seismic hazard analysis is defined as a quantification of some characteristic of the ground motion on the given area of interest.

Seismic hazard curve is defined as a graphical curve depicting the frequency, with which selected values of a seismic hazard such as ground motion amplitude are expected to occur, or more typically, are expected to be exceeded.

Seismic risk is defined as a probability of occurences of the damage and/or loss of lives on the given area of interest due to the seizmic hazard.

Aleatory uncertainty is defined as an uncertainty due to the probabilistic character of the phenomenon. We can´t reduce it by any known methods. Examples are the future position of the earthquake or its size. In the seismic hazard analysis we deal with aleatory uncertainties by probability distribution models.

Epistemic uncertainty is defined as an uncertainty due to the incomplete knowledge of the phenomenon or the parameter of the model of the phenomenon. It can be reduced by improvement of the information about the phenomenon. Examples are the geometry of the seismotectonic and seismogenic zones, median value of ground motion given the source properties and the distributions describing source parameters such as maximum potential magnitude. In the seismic hazard analysis we deal with epistemic uncetainties by the logic tree method.

Uncertainty is a general term for both aleatory and epistemic uncertainty.

Deaggregation is defined as a statistical distribution of the seismic hazard into relative contributions of the particular seismic sources due to magnitude, distance and variations of the seismic motion.

The notions „seismic hazard“ and „seismic risk“ are often incorrectly interchanged, mainly by non-seismologists. The difference between them is slight: the term „seismic hazard“ characterizes the seismic motion on the area of interest regardless the results caused, while the term „seismic risk“ directly refers to the consequences of the seismic motion on the structures and living beings. High level of seismic activity on the area of interest can create high seismic hazard but low seismic risk at the same time (e.g Atacama desert) or subsequently the areas with low seismic hazard can have high levels of seismic risk (e.g due to low quality of the buildings).

1.2 Ground motion characteristics

Seismic ground motion can be according to Kramer (1996) characterized by following quantities:

- Time histories, i.e seismograms, velocigrams and accelerograms
- Physical quantities derived from time histories:
    - PGA (peak ground acceleration)
    - PGV (peak ground velocity)
    - CAV (cumulative absolute velocity)
    - Arias intensity
    - A_{RMS} (root mean square acceleration)
    - PDA (peak differential acceleration)
- Response spectra
- Macroseismic intensity

Time histories fully characterize the seismic ground motion on the area of the interest. They are hard to determine, that´s why following derived characteristics are used:

Peak ground acceleration, which is defined as

$$PGA(x) = \underset{t}{Max}[a(x,t)], \tag{1.1}$$

where *a(x,t)* is an accelerogram recorded at site *x* in the time *t*.

Peak ground velocity, which is defined as

$$PGV(x) = \underset{t}{Max}[v(x,t)], \tag{1.2}$$

where *v(x,t)* is a velocigram recorded at site *x* in the time *t*.

Cumulative absolute velocity, is simply the area under the absolute accelerogram

$$CAV(x) = \int_0^{t_{max}} |a(t)| dt, \tag{1.3}$$

Arias intensity, which is defined as

$$I_A = \frac{\pi}{2g}\int_0^{T_d} a^2\,(x,t)dt, \tag{1.4}$$

where g is gravitational acceletaration and T_d is total duration time of the motion above a given threshold.

Peak differential acceleration, which is defined as

$$PDA(x) = \underset{t}{Max}\left(\frac{\partial a(x,t)}{\partial x}\right). \tag{1.5}$$

Duration of a strong ground motion, which can be described using different approaches. The bracketed duration (Bolt, 1969) is defined as the time between the first and last exceedances of a threshold acceleration (usually 0.05*g*). Another definition (Trifunac and Brady, 1975) is based on the time interval between the points at which 5% and 95% of the total energy has been recorded.

Root mean square acceleration, which is defined as

$$A_{RMS}(x) = \sqrt{\frac{O{,}9}{Td(x)}\int_0^{\infty} a^2(x,t)}, \tag{1.6}$$

where $T_d(x)$ is the duration of a strong ground motion and $a(x,t)$ is the acceleration measured at site x in the time t.

Response spectrum describes the maximum response of a single-degree-of-freedom (SDOF) system to a particular input motion as a function of the natural frequency (or natural period) and damping ratio of the SDOF system. Response spectrum represents the interaction of the building and the bedrock

1.3 Macroseismic intensity

Macroseismic intensity is used to characterize the macroseismic (non-instrumental) effects of the earthquakes on people, buildings and nature. It is typically used for quantification of the effects of historical earthquakes, when it is impossible to use magnitude. The advantage of the macroseismic intensity is the fact, that it is relatively easy to use. Disadvantage of macroseismic intensity are unclear boundaries between given intensity degrees and therefrom resulting higher uncertainty.

In the praxis, macroseismic intensity scales are used. Every intensity scale has some given number of degrees, most common number of degrees being 12. Every degree is characterized by a set of observed signs which fully describes the effects of the earthquake of the given macroseismic intensity.

1.3.1 History of macroseismic intensity

Historically, many intensity scales were developed. Some of the currently used intensity scales are:

- Modified Mercalli intensity scale (MMI), which is used mainly in the USA,
- Mercalli-Cancani-Sieberg intensity scale (MCS), which is used mainly in Italy,
- Medvedev-Sponheuer-Kárnik intensity scale (MSK), which is used mainly in France,
- European macroseismic scale (EMS-98).

All of these intensity scales have 12 intensity degrees. There are other intensity scales which have different number of degrees, for example the Japanese intensity scale (JMA) uses 7 intensity degrees.

History of macroseismic intensity by years (Musson et al., 2009):

- 1783: First simplified usage of macroseismic intensity scales (Schiantarelli).
- 1828: First usage of intensity scales (Egen).
- 1883: The first globally used intensity scale appear (Rossi-Forel intensity scale).
- 1902: Mercalli modified Rossi-Forel scale.
- 1904: Cancani modified Mercalli scale (Forel-Mercalli scale).
- 1912: Sieberg rewrote Cancani scale.
- 1923: New version of Sieberg scale.
- 1931: Wood and Neumann translated Sieberg intensity scale from German to English. This scale is sometimes called Modified Mercalli scale (MMI).
- 1956: Richter developed „Modified Mercalli scale of 1956“ (MM56).
- 1964: First version of MSK, based on MCS and MM56.
- 1988: The revision of MSK is agreed by European seismological comission.
- 1993: Short version of the revision is developed. A preliminary EMS scale was proposed (EMS-92).
- 1998: Full version of the revision is developed, under the supervision of Gottfried Grünthal (EMS-98).

The fact that the macroseismic intensity scales are not equal has to be everytime taken into account. The interchanging of the intensity scales without deeper research of the relations between them would create considerable error. The most precise way of dealing with this error is to review the original macroseismic reports. They are however not always available. In this case we can use the conversion table for macroseismic intensities (Musson et al., 2009). The table is presented in Fig. 1.

RF	EMS-98	MCS	EMS-98	MMI 56	EMS-98	MSK	EMS-98	JMA-96	EMS-98
								0	1
1	1	1	1	1	1	1	1	1	2 or 3
2	2	2	2	2	2	2	2	2	4
3	3	3	3	3	3	3	3	3	4 or 5
4	4	4	4	4	4	4	4	4	5
5	5	5	5	5	5	5	5	5L	6
6	5	6	6	6	6	6	6	5U	7
7	6	7	7	7	7	7	7	6L	8
8	7 or 8	8	8	8	8	8	8	6U	9 or 10
9	9	9	9	9	9	9	9	7	11
10	*	10	10	10	10	10	10		
		11	11	11	*	11	11		
		12	*	12	*	12	*		

Fig. 1: Conversion table of different macroseismic intensity scales (source: Musson et al., 2009).

1.3.2 European macroseismic scale EMS-98

European macroseismic scale is the set of classifications of the earthquakes from different points of view. It contains the descriptions of the particular intensity degrees, the classification of the buildings by their vulnerability, classification of the damages etc.

The buildings are divided into 6 vulnerability classes (A-F) - A is the most vulnerable and F is the least vulnerable. The vulnerability is specified by the material, the building is made of. The most buildings in Slovakia are from classes A-C. The table of different vulnerability classes is presented in Fig. 2.

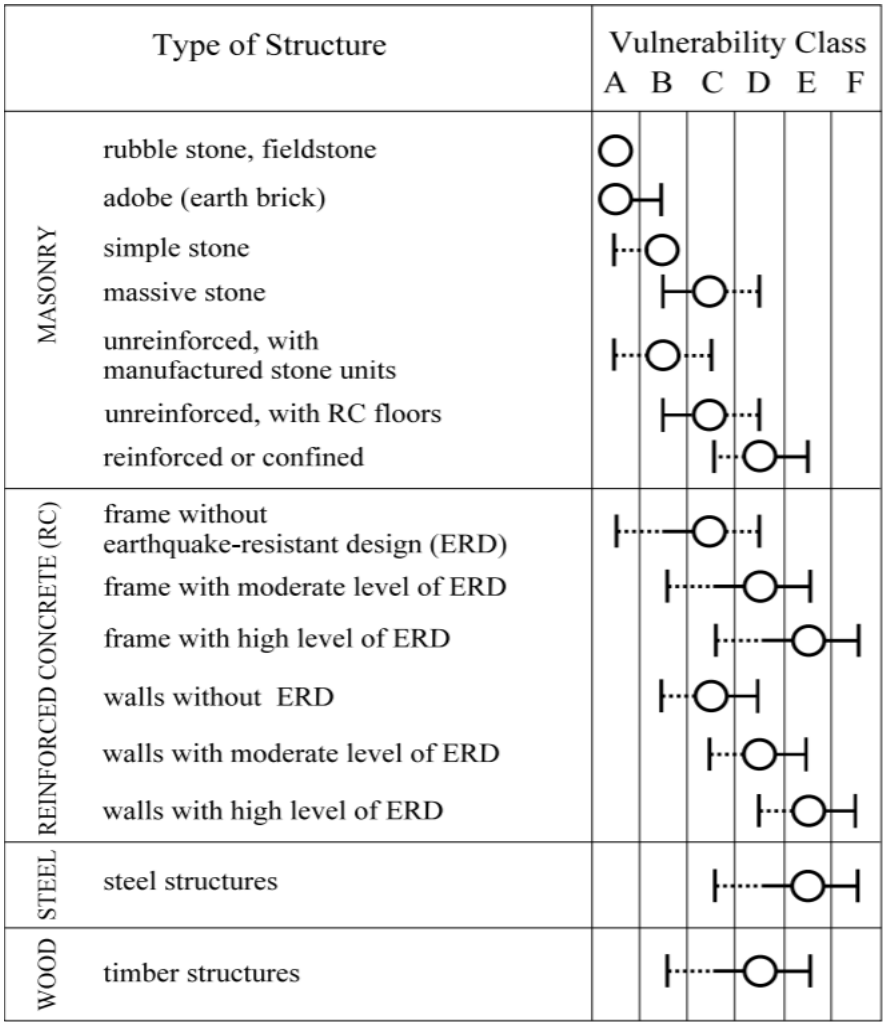

Fig. 2: Vulnerability classes of the buildings according to EMS-98 (source: Grünthal, 1998).

The intensity scale also divides damages into five categories:

1. Negligible to slight damage (no structural damage, slight non-structural damage)
2. Moderate damage (slight structural damage, moderate non-structural damage)
3. Substantial to heavy damage (moderate structural damage, heavy non-structural damage)
4. Very heavy damage (heavy structural damage, very heavy non-structural damage)
5. Destruction (very heavy structural damage)

The definitions of quantity (few, many, most) are frequently used in EMS-98. Each of them represents some percentage and helps with further definitions and descriptions. The definitions of quantity are presented in Fig.3.

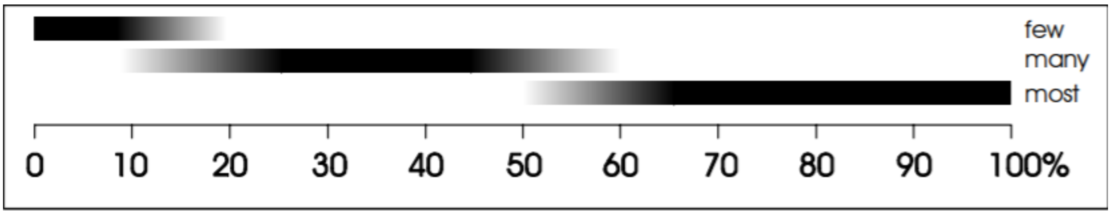

Fig. 3: Definitions of quantity presented in EMS-98 (source: Grünthal, 1998).

Intensity degrees are classified with respect to three effects of the earthquakes:

a) Effects on humans
b) Effects on objects and nature
c) Damage to buildings

By these three effects we can divide the earthquakes into 12 intensity degrees. The intensity degree 1 is also called as „no earthquake“ and intensity degree 12 is only theoretical. The following two intensity degrees examples are cited from Grünthal (1998).

III. Weak

a) The earthquake is felt indoors by a few. People at rest feel a swaying or light trembling.
b) Hanging objects swing slightly.
c) No damage.

VI. Slightly damaging

a) Felt by most indoors and by many outdoors. A few persons lose their balance. Many people are frightened and run outdoors.
b) Small objects of ordinary stability may fall and furniture may be shifted. In few instances dishes and glassware may break. Farm animals (even outdoors) may be frightened.

c) Damage of grade 1 is sustained by many buildings of vulnerability class A and B; a few of class A and B suffer damage of grade 2; a few of class C suffer damage of grade 1.

1.4 Methods of seismic hazard analysis

The information used in this subchapter are mainly from Reiter (1990).

The seismic hazard analysis is made in two steps:

1. Identification and characterization of seismic source zones
2. Determination of ground motion characteristic on the area of interest

There are two main approaches of seismic hazard analysis – deterministic seismic hazard analysis (DSHA) and probabilistic seismic hazard analysis (PSHA).

Before the analysis, it is needed to compile the input databases for the area of the interest. They consist of geological, seismological, geophysical and geotechnical data about the area of interest and region.

The most important data in the seismological database are date, time and size of earthquake, the position of epicentre and/or hypocentre, epicentral intensity of the earthquake, the description of observed damages, records from seismographs, the information about foreshocks and aftershocks and information about the causative fault.

1.4.1 Deterministic seismic hazard analysis

Deterministic seismic hazard analysis (DSHA) is that which, for most part, uses single-valued events or models to arrive at scenario-like descriptions of seismic hazard. This analysis requires the specification of three basic elements: an earthquake source (fault Y), a controlling earthquake of specified size and a means of determining the hazard at the specified distance to the site.

DSHA can be described as a four-step process (Fig. 4):

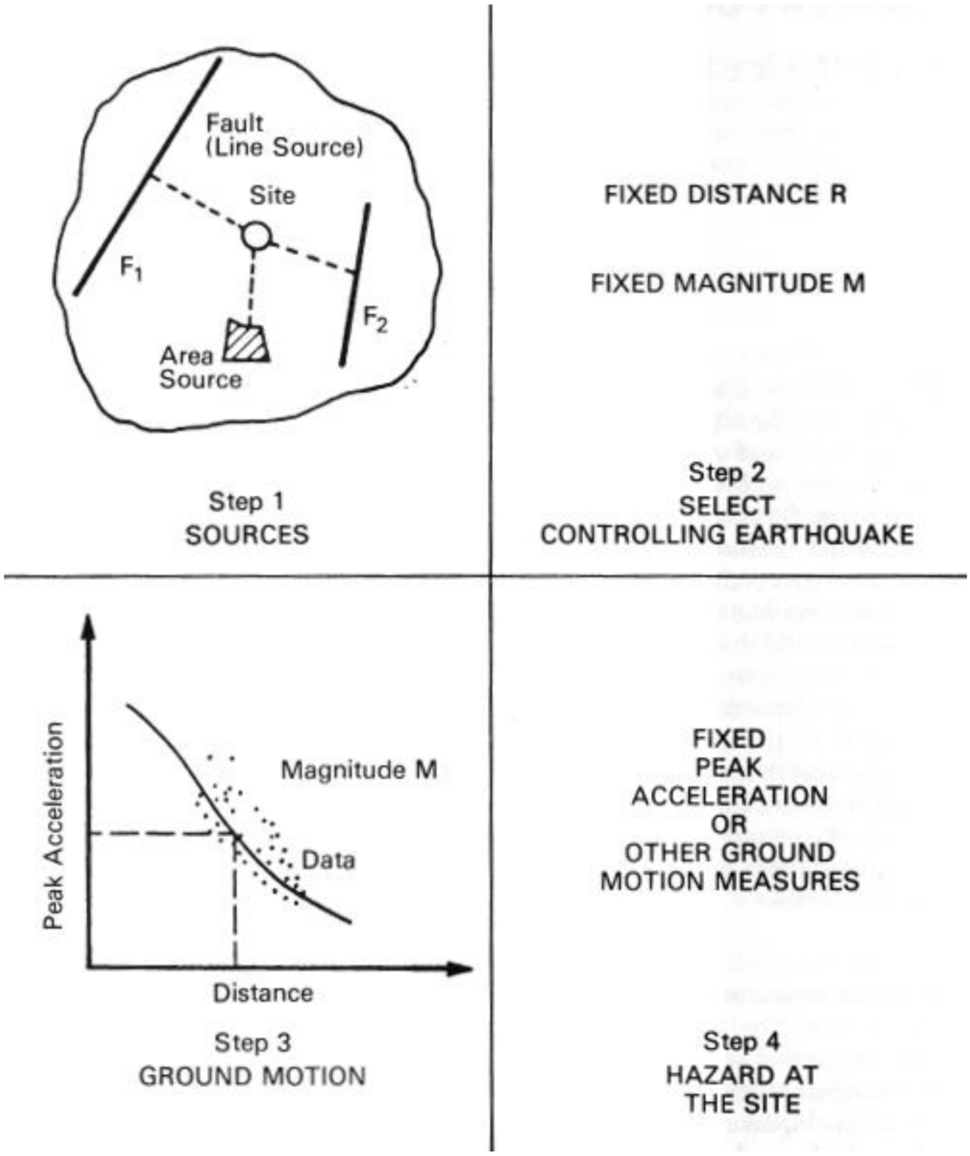

Fig. 4: Four steps of deterministic seismic hazard analysis (source: Reiter, 1990).

1. step: Definition of an earthquake source

In this step, we identify and allocate seismic source zones (point, linear, surface and volumetric) using compiled geophysical databases.

2. step: Selection of the controlling earthquake

We determine the maximum earthquake for every seismic source zone. The maximum potential earthquake is characterized by epicentral intensity or magnitude. For every seismic source zone we determine the minimum distance from source to site. If the site is located in the seismic source zone, we assume the occurence of the maximum potential earthquake under the locality. Controlling earthquake is then the earthquake, which characteristics (ground motion and/or other quantities) are dominant in comparision with maximum potential earthquakes from other seismic source zones.

3. step: Determinition the earthquake effect

In this step we use empirically derived ground motion prediction equations (GMPEs) for chosen ground motion characteristic. They allow us to determine the seismic hazard on the area of interest.

GMPEs, previously known also as attenuation relations, can be divided to equations for stable continental regions, active shallow crustal regions, vulcanic regions, subduction zones and for deep-focus earthquakes.

GMPEs contain mostly terms, which characterize the attenuation of the ground motion characteristic depending on the distance from the source of the earthquake.

GMPE is an empirical relation which standardly has form

$$lnY = g(m, r, s_i) + \varepsilon, \tag{1.7}$$

where *Y* is the selected ground motion characteristic,

$g(m,r,s_i)$ is the function which expresses the dependence of the selected characteristic on the magnitude *m*, distance *r* and other important parameters s_i such as local geological conditions

and ε is a random variable corresponding to the aleatory uncertainty. We assume that ε has normal (Gaussian) distribution with mean equal to zero and standard deviation (σ).

For example, GMPE Boore et al. (1997) has a functional form:

$$lnY = b_1 + b_2(M - 6) + b_3(M - 6)^2 + b_5 \ln r + f, \tag{1.8}$$

where *Y* is the selected ground motion characteristic and *M* is the moment magnitude. In the equation, we can see the term linearly and quadratically dependent on the magnitude $b_2 (M\text{-}6)+b_3 (M\text{-}6)^2$ and the term dependent on the distance $b_5 \ ln \ r$. The term *f* defines the local characteristics of the area of interest. Parameters b_1, b_2, b_3, b_5 are determined by regression from the strong ground motion data.

List of all published GMPEs can be found in Douglas (2016).

When the ground motion characteristic *Y* is macroseismic intensity, the equation

$$\ln I = g(m, r, s_i) + \varepsilon, \tag{1.9}$$

is called intensity prediction equation (IPE). There is other frequently used type of IPEs, which has a form:

$$dI = I_0 - I = g(r, s_i) + \varepsilon, \tag{1.10}$$

where I_0 is epicentral intensity.

4. step: Determination of the seismic hazard at the site

By using suitably chosen ground motion prediction equations, we determine the effects of the controlling earthquake at the site.

The greatest advantage of DSHA is that it is relatively simple to use. It provides the evaluation of worst-case scenario of ground motion without knowing the likelihood of occurence of the controlling earthquake.

The problem of DSHA is that we are not always able to determine the worst-case scenario and we also need to account for uncertainties.

1.4.2 Probabilistic seismic hazard analysis

Probabilistic seismic hazard analysis (PSHA) uses statistical methods for computation of probability of exceeding the threshold value of ground motion characteristic at the site for chosen time period. It incorporates the effects of all earthquakes from all distances that affect the seismic hazard at the site.

The outcome of PSHA is the expected frequency of exceedances of chosen ground motion characteristic per time unit. Other form of outcome of PSHA is the seismic hazard curve, which expresses the probability of exceedance of chosen ground motion characteristic per time unit. The outcomes of PSHA are used mainly in engineering and in seismic risk determination.

Similarly to DSHA, PSHA consists of four steps (Fig. 5):

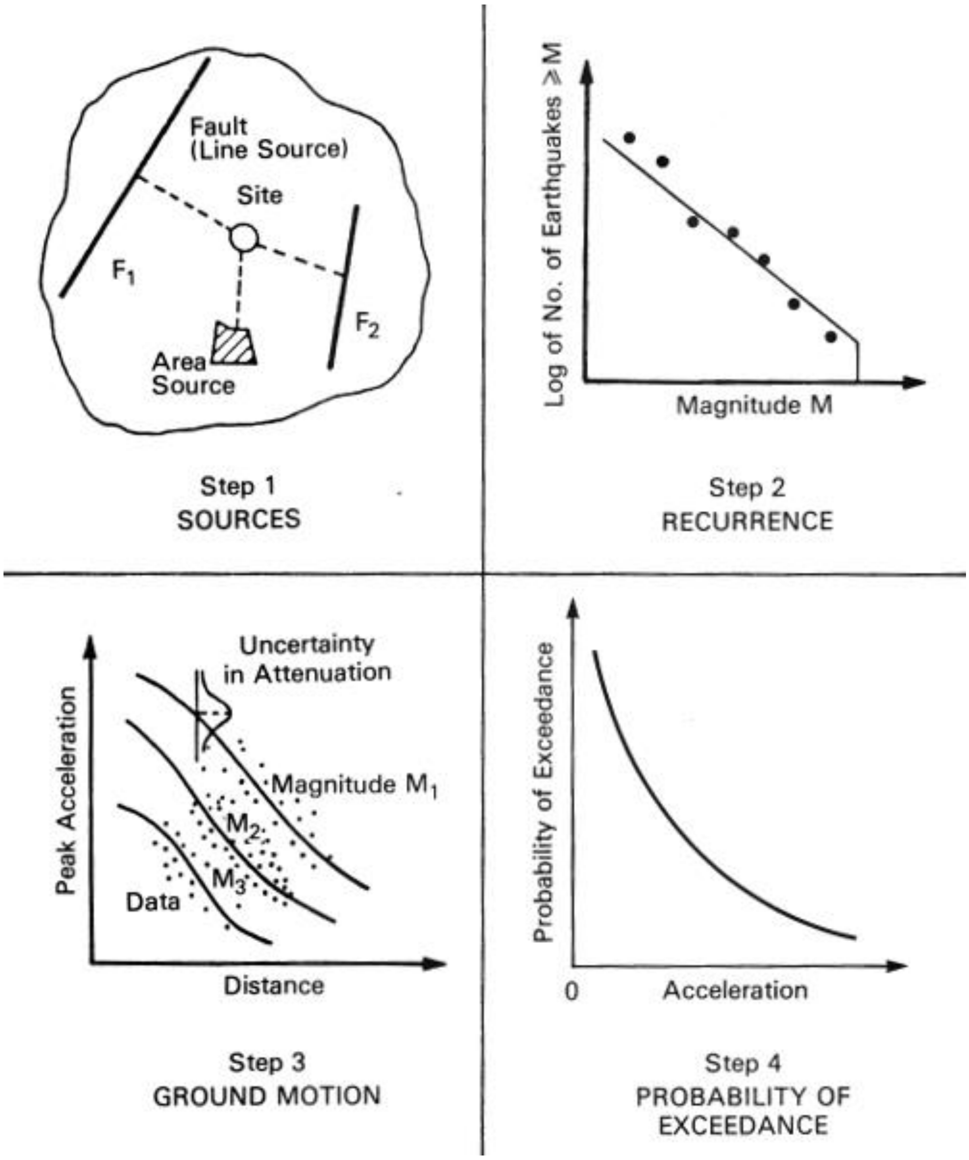

Fig. 5: Four steps of probabilistic seismic hazard analysis (source: Reiter, 1990).

1. step: Identification of seismic source zones

Similarly to DSHA, we identify seismic source zones using compiled geological, seismological and geophysical databases. The seismic activity is in the case of PSHA considered to be spatially homogenous.

2. step: Determination of magnitude-frequency relations

For every seismic source zone we determine magnitude-frequency relation and maximum potential magnitude. The magnitude-frequency relation expresses the number of earthquakes per time unit at the site and according to Gutenberg and Richter (1944) it has a form

$$\log(n) = a - bM, \qquad (1.11)$$

which can be expressed also as

$$n(M) = \alpha . e^{-\beta M}, \alpha = 10^a, \beta = b . \ln 10, \qquad (1.12)$$

where n is the number of the earthquakes with magnitude equal to or higher than M, and α, β, a, b are coefficients given by regression. The parameters a, b, α and β have a physical meaning. Parameter α has a meaning of cumulative number of earthquakes with magnitude larger or equal to 0 per year, therefore $n(0) = \alpha$. Parameter b defines the ratio of number of occurrences of weak to strong earthquakes. The b-value for areas inside of lithospheric plates is typically approximately 1. Lower b-value means higher ratio of occurrences of strong to the weak earthquakes per year. This leads to higher seismic hazard, mostly for long return periods.

Since the equations (1.12) describe the exponential distribution and the relation between epicentral macroseismic intensity and magnitude is linear, we can exchange magnitude for macroseismic intensity. Then the equation (1.11) becomes

$$\log(n) = a - bI_0. \qquad (1.13)$$

The coefficients α, β, a, b have a physical meaning. The parameters α and a express the number of earthquakes with magnitude/intensity higher than or equal to 0 (therefore $n(0)= \alpha$) and coefficients β, b describe the ratio of occurences between weak and strong earthquakes in the given seismic source zone.

3. step: Selection of GMPEs

This step is identical to the third step in deterministic seismic hazard analysis, which was described in subchapter 1.4.1.

4. step: Determination of the seismic hazard at the site

The seismic hazard at the site is determined by computation of seismic hazard integral, which is analyzed in subchapter 1.4.3.

The outcome of the PSHA is probability of exceedance of ground motion characteristic threshold. We often use 10% probability of exceedance of peak ground acceleration in 50 years or 1% probability of exceedance in 100 years.

Optional 5. step: Deaggregation

Deaggregation is an optional step of PSHA. It describes how earthquakes of various magnitudes from various distances contribute to the resulting seismic hazard. It is a form of statistical decomposition. The outcomes are the values of computed ground motion chaarcteristic for pairs magnitude-distance.

1.4.3 Mathematical description of probabilistic approach

The probability of exceedance of chosen threshold *c* of ground motion characteristic *C* on the area of interest *P(C > c)* can be computed by so called seismic hazard integral (Baker, 2013).

$$P(C > c) = \int_{Mmin}^{Mmax} \int_{0}^{Rmax} P(C > c|m, r) f^R(r)\, f^M(m) dr dm, \qquad (1.14)$$

where

$P\ (C > c)$	is the probability of exceedance of chosen threshold c of ground motion characteristic C at the area of interest,
M_{min}	is the minimum considered magnitude,
M_{max}	is the maximum potential magnitude,
R_{max}	is the maximum considered distance of seismic source zone,
$f^R\ (r)$	is the probability density function of distribution of source-to-site distances,
$f^M\ (m)$	is the probability density function of distribution of earthquake magnitudes,
$P\ (C > c\|m,r)$	is the probability, that the earthquake at distance r with magnitude m will exceed threshold c of the ground motion characteristic C.

Minimum considered magnitude is chosen so that it already causes damage of buildings, typically between 4.5 and 5.0. It is chosen by seismic engineers.

Maximum potential magnitude is the largest possible earthquake on the seismic source zone. However, it is not equal to the largest observed magnitude in the given seismic source zone. Often we consider the largest observed magnitude unit with some small added value (e.g. 0,5-1 magnitude) as maximum potential magnitude.

In seismic hazard analysis, it is very important to know the expected number of exceedances per year of chosen threshold c of ground motion characteristic C ($N(C > c)$), which can be computed as follows

$$N\ (C > c) = \lambda^{min} P(C > c), \tag{1.15}$$

where λ^{min} is the number of earthquakes with magnitude greater than M_{min} per year.

Then formulas (1.14) and (1.15) can be merged into

$$N(C > c) = \lambda^{min} \int_{Mmin}^{Mmax} \int_{0}^{Rmax} P(C > c|m, r) f^{R}(r)\, f^{M}(m) dr dm. \tag{1.16}$$

Formula (1.16) expresses only the expected number of exceedances of chosen ground motion characteristic per year from one seismic source zone. The expected value of exceedances per year from all seismic source zones can be computed by summation

$$N\ (C > c) = \sum_{j=1}^{J} N_j\ (C > c) \tag{1.17}$$

where $N_j(C > c)$ is the expected number of exceedances per year of chosen ground motion characteristic C from j-th seismic source zone and J is the total number of seismic source zones.

The formula (1.17) can be transformed to form

$$N\ (C > c) = \sum_{j=1}^{J} P_j\ (C > c) \lambda_j^{min}, \tag{1.18}$$

where λ_j^{min} is the number of earthquakes from j-th seismic source zone with magnitude larger than M_{min} per year.

Then finally by merging formulas (1.14) – (1.18) we get the formula

$$N\ (C > c) = \sum_{j=1}^{J} \lambda_j^{min} \int_{Mmin}^{M_j^{max}} \int_{0}^{Rmax} f_j^{R}(r) f_j^{M}(m) P(C > c|m, r)\, dr dm, \tag{1.19}$$

where M_j^{max} is the maximum potential magnitude for j-th seismic source zone,

f_j^R is the probability density function of distribution of source-to-site distances from j-th seismic source zone,

f_j^M is the probability distribution function of distribution of earthquake magnitudes from j-th seismic source zone.

1.5 The application of Poisson process in seismic hazard analysis

The earthquake can be considered as a random Poisson process if these three basic conditions are fulfilled (Kramer, 1996):

1. The number of occurrences in one time interval are independent of the number that occur inany other time interval.
2. The probability of occurence during a very short time interval is proportional to the length of the time interval.
3. The probability of more than one occurence during a very short time interval is negligible.

This consideration is often used in probabilistic approach. It is very important, that foreshocks and aftershocks are in a conflict with the first and the second condition, so it is neccessary to identify them and remove from the seismic hazard computation. This is called *earthquake catalogue declustering* and it will be further analyzed later.

If we consider earthquakes to be independent phenomena, which don´t occur at the same time, the occurrence of earthquakes can be described by Poisson distribution which has the form

$$P(C > c|T) = 1 - e^{-N(C>c)T}, \quad (1.20)$$

where $P(C > c|T)$ is the probability of exceedance of chosen threshold c of ground motion characteristic C on the area of interest during the time period of T years.

Then *return period* is the time period, during which at least one exceedance of chosen threshold c of ground motion characteristic C occurs. It can be determined by logarithming of the formula (1.20) and has the form

$$RP = \frac{-T}{\ln(1-P(C>c))}. \quad (1.21)$$

In praxis, 10% probability of exceedance of chosen threshold c of ground motion characteristic C on the area of interest during the time period of 50 years is often used. The return period in this case is 475 years.

1.6 Discussion of physical meanings of terms in seismic hazard integral

M_{min} – *minimum considered magnitude*

Minimum magnitude is often chosen so that it already can cause damage on buildings. However, the value of the magnitude itself is not the best way of expressing the potential of damages and in the past not enough attention was given to its selection.

M_j^{max} – *maximum potential magnitude for j-th seismic source*

It is the largest earthquake, that can occur in *j*-th seismic source . The brief overview of currently used ways of determining the maximum potential magnitude can be found in Wiemer et al. (2009).

Because the time period of observations of earthquakes is short (the history of earthquakes in catalogues is typically of the order of centuries), maximum potential magnitude does not equal the largest observed magnitude. We can consider the largest observed magnitude plus some small additive value (typically 0.5 or 1.0) to be the maximum potential magnitude.

Maximum potential magnitude can be determined from the estimations of the maximum length of rupture and/or displacements caused by future earthquakes by empirical relations.

f_j^R – *probability density function of distribution of distances between j-th seismic source and the area of interest*

This term is the result of dividing the area of interest into seismic sources. It is therefore affected by seismic source zones, their geometry and position of area of interest with respect to seismic source zone.

f_j^M – *probability density function of distribution of magnitude for j-th seismic source*

This term is determined by magnitude-frequency relation. In most cases we use Guttenberg-Richter type of magnitude-frequency relation (1.10) which can be expressed as (1.11).

The magnitude *m* for seismic source *j* is typically from the interval

$$M_j^{max} \geq m \geq M^{min}. \tag{1.22}$$

The upper boundary of the interval is given by maximum potential magnitude. The value of maximum potential magnitude is given by rupture length, it is the strongest magnitude that can be caused by a rupture of a known length. The lower boundary M^{min} is given by „quality" of the earthquake catalogue, mostly by its time completeness for small magnitudes.

For such bounded magnitude interval of earthquakes, we can derive so called double-truncated magnitude-frequency relation

$$n(m) = \alpha^{min}(1 - \frac{1-e^{-\beta(m-Mm)}}{1-e^{-\beta(M_j^{max}-Mm)}}), \quad (1.23)$$

where α^{min} is the number of earthquakes with magnitude *m* in interval $M_j^{max} \geq m \geq M^{min}$ per year. The respective probability density function of distribution for *j*-th seismic source can be expressed (McGuire, 2004) as

$$f_j^M(m) = \beta \frac{e^{-\beta(m-M^{min})}}{1-e^{-\beta(M_j^{max}-M^{min})}}, \quad (1.24)$$

which is used in formula (1.18).

λ_j^{min} – *the number of earthquakes from jth source with magnitude greater than* M_{min}

From (1.23) we can show that

$$\alpha^{min} = \lambda_j^{min}. \quad (1.25)$$

$P(C > c|m,r)$ – *probability, that earthquake with magnitude m at the distance r will exceed threshold c of ground motion characteristic C*

This probability can be determined by GMPE. We are interested in cases, when

$$C > c; \quad \ln C > \ln c; \quad g(m,r) + \varepsilon > \ln c; \quad \varepsilon > \ln c - g(m,r), \quad (1.26)$$

is valid.

Then we can compute

$$P(C > c|m,r) = P(\varepsilon > \ln c - g(m,r)|m,r)$$

(1.27)

$$= \int_{\ln c - g(m,r)}^{\infty} \frac{1}{\sigma\sqrt{2\pi}} e^{-\frac{\varepsilon^2}{2\sigma^2}} d\varepsilon$$

$$= 1 - \int_{-\infty}^{\ln c - g(m,r)} \frac{1}{\sigma\sqrt{2\pi}} e^{-\frac{\varepsilon^2}{2\sigma^2}} d\varepsilon$$

$$= 1 - \phi(\frac{1}{\sigma}\left(\ln c - g(m,r)\right),$$

where ϕ is the standard normal cumulative distribution function.

Desired probability, that earthquake with magnitude *m* at the distance *r* will exceed threshold *c* of ground motion characteristic *C* is then:

$$P(C > c|m,r) = 1 - \phi(\frac{1}{\sigma}\left(\ln c - g(m,r)\right). \quad (1.28)$$

Also the earthquakes with strong ground motion from the margins of the Gaussian distribution of uncertainties for given GMPE contribute to the total seismic hazard, we typically use the truncation of the distribution of ground-motion residuals of GMPE at some multiple of its standard deviation (σ). According to Bommer et al. (2004), when the distribution of aleatory uncertainty in GMPE is not truncated, the seismic hazard, mainly for small number of exceedances of chosen ground motion characteristic per year can be overeatimated (for long return periods).

2 Previous probabilistic seismic hazard analyses of the Slovak territory in terms of macroseismic intensity

In the past, several seismic hazard analyses, which included the Slovak territory were made. Most of them present outcomes in terms of peak ground acceleration, but some of them also utilize macroseismic intensity.

The first probabilistic seismic hazard analysis of Slovakia was the map developed within the project Global Seismic Hazard Assessment Program – GSHAP (Schenk et al., 2000). The goal of this project was to develop global seismic hazard map in terms of peak ground acceleration and macroseismic intensity.

The analysis was conducted region by region and the Slovak territory was analyzed together with the territory of Poland and Czech Republic. The earthquake catalogue Schenková et al. (1999) was used.

The outcome of the project GSHAP for the Slovak territory – seismic hazard map in terms of macroseismic intensity for 90% probability of non-exceedance in 50 years is presented in Fig. 6.

The map shows the highest levels of seismic hazard for the areas of seismic source zone Komárno and seismic source zone Žilina. That corresponds to the location of the 1763 and 1783 Komárno historical earthquakes with macroseismic intensities VIII - IX MSK-64 and the 1858 Žilina earthquake with macroseismic intensity VII - VIII MSK-64.

The second important probabilistic seismic hazard analysis of the Slovak territory was the analysis conducted during preparation of the new national annex to EUROCODE8 (Kysel et al., 2014). This analysis was conducted in terms of peak ground acceleration for return period of 475 years (10% probability of exceedance of peak ground acceleration in 50 years) and was later converted to macroseismic intenstity by using of so called ground motion to intensity conversion equations (GMICE) in Šugár (2016).

The basic form of GMICE resembles equation (1.13):

$$I = a.\log PGA + b, \tag{2.1}$$

so we can see that this equation provides direct conversion of peak ground acceleration into macroseismic intensity. The outcome in terms of peak ground acceleration are presented in Fig. 7 and in terms of macroseismic intensity in Fig. 8.

As we can see, due to the different seismotectonic model, this maps shows the highest levels of seismic hazard for slightly different areas than GSHAP map. The seismic hazard in Komárno source zone is the same, but this map shows moderate levels of seismic hazard for the area of Žilina and higher levels for the area of seismic source zone Dobrá Voda near Trnava. That corresponds to the location of the strongest earthquake in Slovakia in the 20th century – 1906 Dobrá Voda earthquake with macroseismic intensity VIII – IX MSK-64.

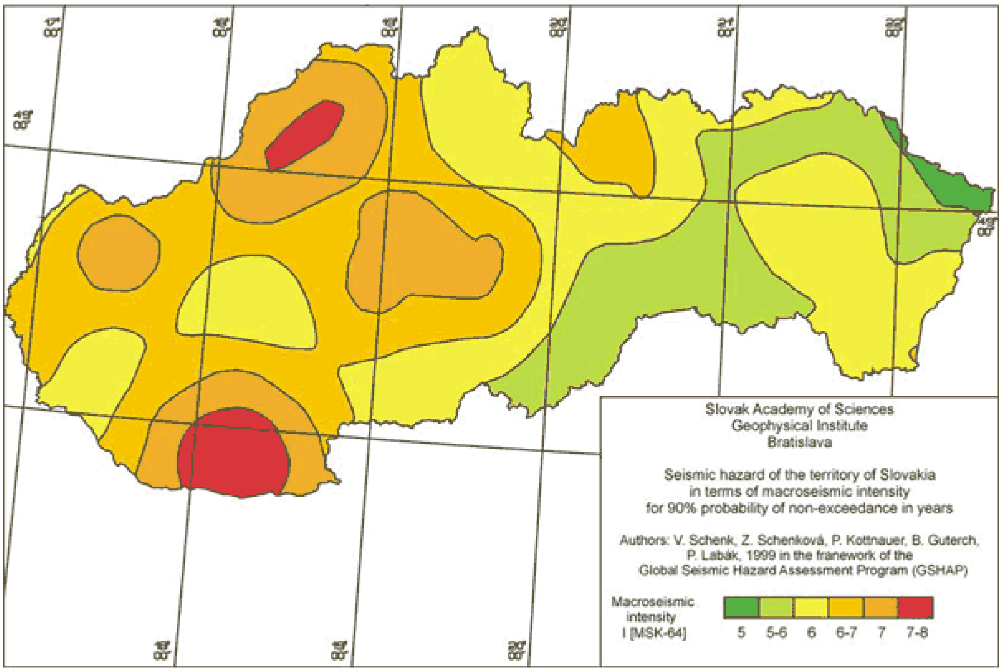

Fig. 6: Seismic hazard map in terms of macroseismic intensity constructed as the outcome of the project GSHAP (source: Schenk et al., 2000).

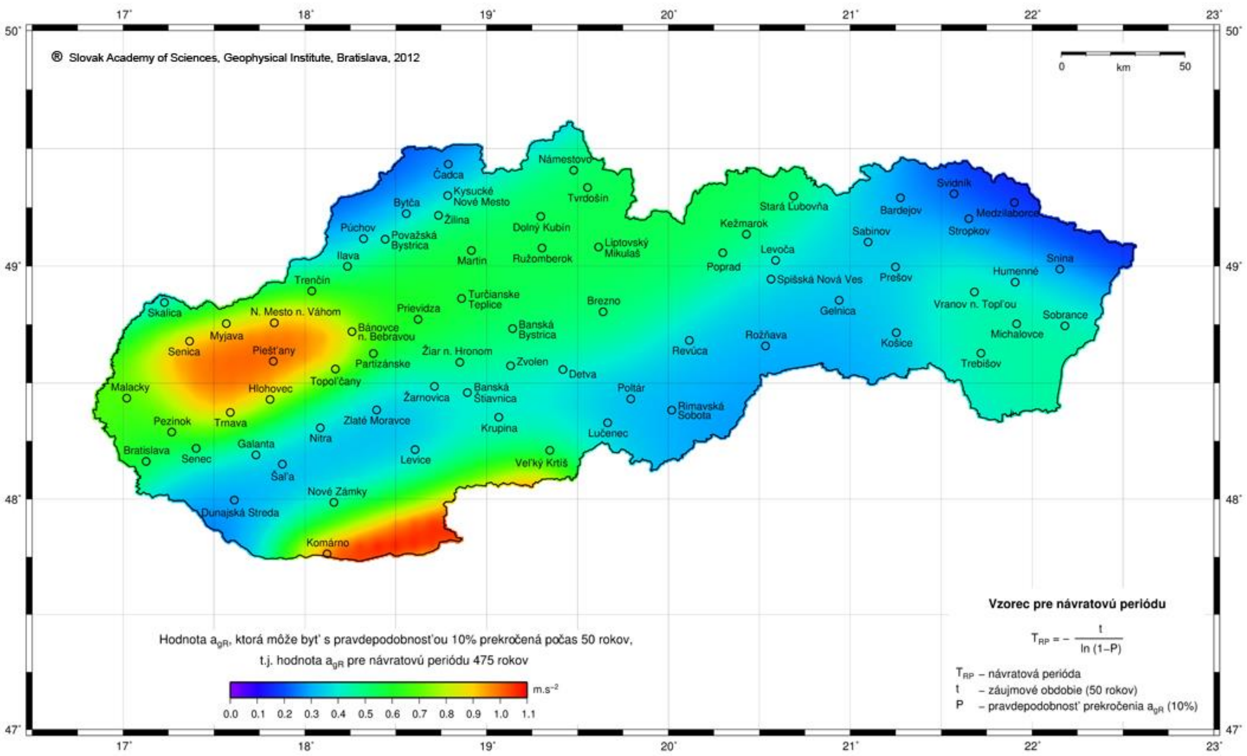

Fig. 7: Seismic hazard map in terms of peak ground acceleration, conducted during preparation of the new national annex of EUROCODE8 (source: Kysel et al., 2014).

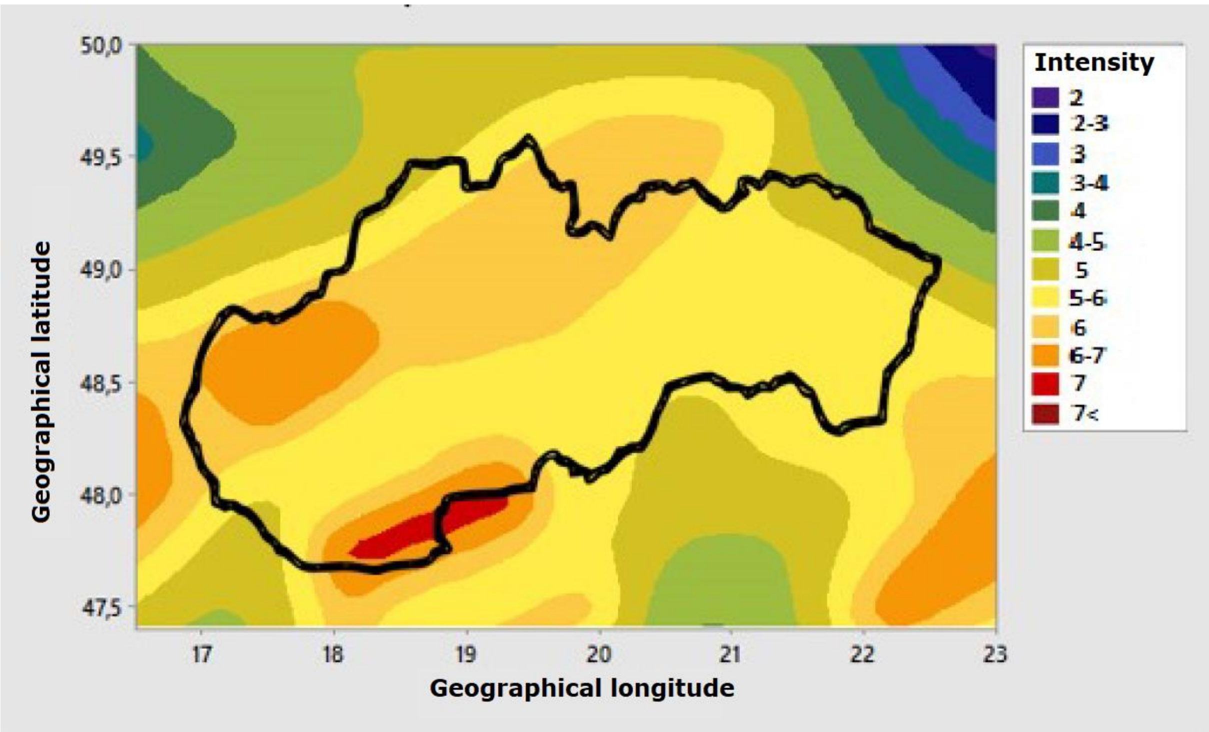

Fig. 8: Seismic hazard map in terms of macroseismic intensity using GMICE (source: Šugár, 2016).

3 Objectives of master´s thesis

The main objective of the master´s thesis is to apply classical probabilistic seismic hazard analysis approach to create seismic hazard map of Slovakia in terms of macroseismic intenstity.

For achieving the main objective, the following partial objectives are needed to fulfill:

1. Compilation of earthquake catalogue for Slovakia and neighbouring countries in terms of macroseismic intensity.
2. Homogenization of the earthquake catalogue.
3. Identification of foreshocks, mainshocks and aftershocks – declustering.
4. The completeness analysis of the catalogue.
5. Determination of intensity-frequency relation and maximum potential intensity for every seismic source zone.
6. Selection of intensity prediction equations.
7. Perform a PSHA computation and analyse the sensitivity of results to input parameters.

4 Earthquake catalogue for Slovakia

The earthquake catalogue is together with geological database an essential input for the development of the seismotectonic model of the area of interest and the determination of parameters of seismic source zones.

4.1 Compilation of earthquake catalogue for Slovakia

We compiled the new earthquake catalogue for the Slovak territory and nearby areas of neighbouring countries for the purpose of the probabilistic seismic hazard analysis of the Slovak territory. During the compilation, following earthquake catalogues were used:

- Catalogue of the Geophysical Institute of Slovak Academy of Sciences (GPI SAS, 2012)
- Hungarian national catalogue Zsíros (2000)
- Catalogue of the Geophysical Institute of the Czech Academy of Sciences (GPI CAS, 2005)
- Regional catalogue ACORN (2004)
- The European-Mediterranean earthquake catalogue (EMEC, 2012)
- Austrian national catalogue (ZAMG, 2011)
- The catalogue for territory of Poland (Pagaczewski, 1972)

The basic summary of used catalogues is shown in Tab. 1.

Catalogue	GPI SAS (2012)	Zsíros (2000)	GPI CAS (2005)	ACORN (2004)	EMEC (2012)	ZAMG (2011)	Pagaczewski (1972)
Geographic coverage	AT, CZ, HU, PL, SK	AT, CR, HU, RS, SK, SL	AT, CZ, PL, SK	AT, CZ, HU, SK	AT, CR, CZ, HU, PL, RS SK, SL	AT, CZ, HU, SK	PL
Period	1022 – 2011	456 – 1995	1985 - 2004	1267 – 2004	1000 - 2006	1022 – 2011	1011 – 1966
Type of magnitude	M_L, M_S, MI_O	M_L, M_S, *mb*, *mDur*, MI_O	M_L	M_L, MI_O	M_L, M_S, *mb*, *mDur*, M_W	M_S, M_L, MI_0	MI_0
Macroseismic intensity scale	not specified	EMS – 98	not specified	MSK – 64	not specified	not specified	MCS
Number of events	3431	20 478	1034	1962	3394*	1234	111

Tab. 1: Overview of earthquake catalogues used for compilation of the preliminary earthquake catalogue and type of entry data.

Abbreviations used: AT – Austria, CR – Croatia, CZ – Czech Republic, HU – Hungary, PL – Poland, RS – Serbia, SK – Slovakia, SL – Slovenia, M_L – local magnitude, *mb* – body wave magnitude, M_S – surface wave magnitude, *mDur* – earthquake duration magnitude, MI_0 – magnitude determined from epicentral macroseismic intensity, M_W – moment magnitude.

* - the number of events is only for Slovakia and nearby areas of neighbouring countries.

The preliminary catalogue was merged from listed earthquake catalogues. The 350 Carnuntum intensity IX – X earthquake was also added (Decker, 2006). We excluded the events outside the area of the seismotectonic model SK2011 (Hók et al., 2016). We checked the catalogue for duplicities and excluded them, leaving only one primary entry. The entries from national earthquake catalogues were prioritized. The final earthquake catalogue consists of 3720 entries with macroseismic intensities between II and IX – X for the time period of 350 – 2011.

4.2 Homogenization of earthquake catalogue

The earthquake catalogue was homogenized so that all entries contain also the information about the moment magnitude M_W – uniform physical quantity that fully describes the size of the earthquake.

We considered the epicentral macroseismic intensity from the intensity scale MSK-64 to be equivalent to the epicentral macroseismic intensities in scales EMS-98 and MCS:

$$I_{0\,MSK-64} = I_{0\,EMS-98} = I_{0\,MCS}. \tag{4.1}$$

For the conversion of entries from macroseismic intensity I_0 to moment magnitude M_W without focal depth we used the equation (Grünthal, 2009):

$$M_W = 0.682\, I_0 + 0.16. \tag{4.2}$$

For entries with focal depth we used the equation (Grünthal, 2009):

$$M_W = 0.667\, I_0 + 0.3\, \log_{10} h - 0.1, \tag{4.3}$$

where M_W is the moment magnitude, I_0 is the macroseismic intensity and h is the focal depth.

The time-intensity distribution of earthquakes from homogenized earthquake catalogue is shown in Fig. 9 and the time-intensity distribution of earthquakes from homogenized catalogue after 1900 is shown in Fig. 10. As we can see, the number of earthquakes dramatically increases in the last century. This is caused by the fact, that people started to collect the earthquake data systematically and also instrumentally, therefore it was possible to collect information about earthquakes that were not macroseismically observed.

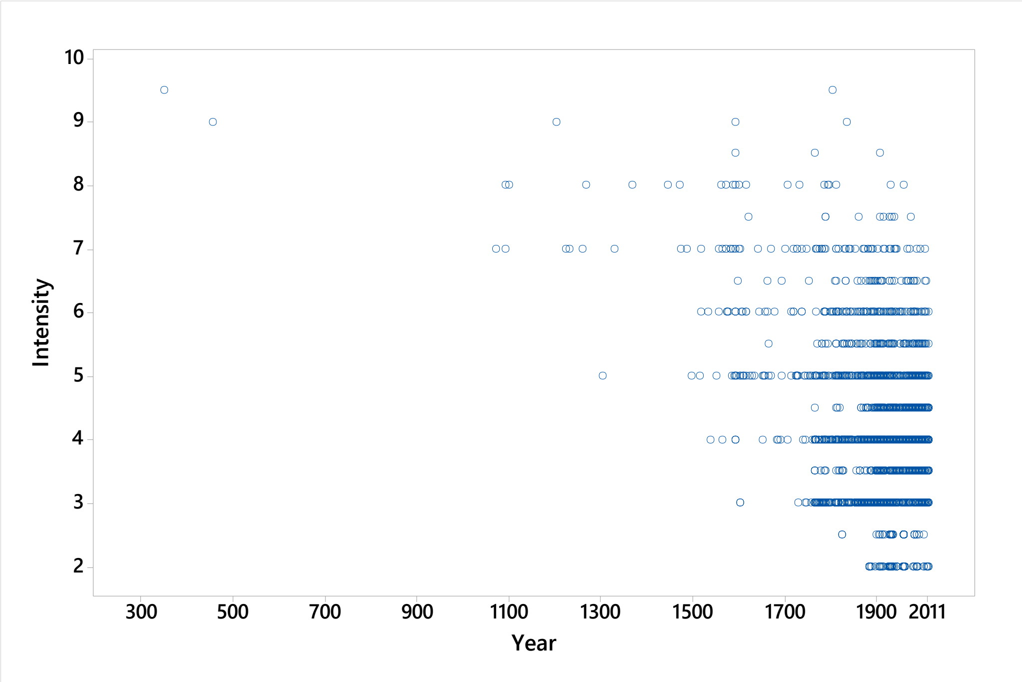

Fig. 9: Time-intensity distribution of earthquakes from homogenized earthquake catalogue.

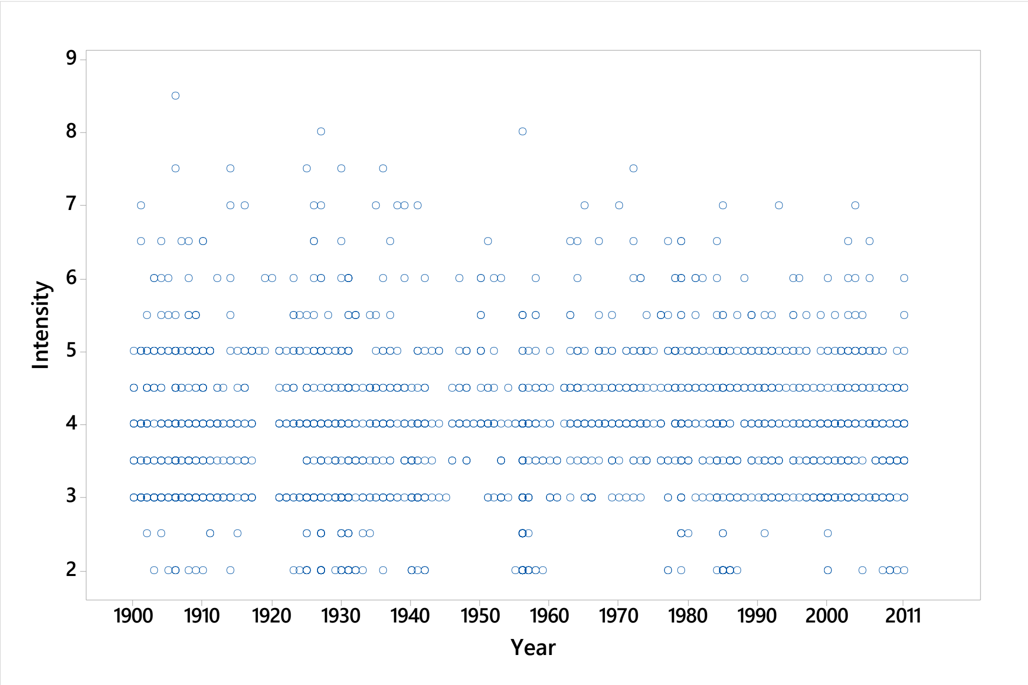

Fig. 10: Time-intensity distribution of earthquakes from homogenized earthquake catalogue after 1900.

4.3 Determination of foreshocks, mainshocks and aftershocks

For determination of the category of an earthquake, i.e. if the event is a foreshock, a mainshock or an aftershock we used two methods – cluster method (Reasenberg, 1985) and window method and we compared the results.

4.3.1 Cluster method

The cluster method links the earthquakes into so called clusters, which sizes grow proportionally with number of processed earthquakes. The earthquakes are linked into clusters depending on spatial and temporal interaction zones. Spatial interaction zones are chosen depending on stress distribution near the mainshock.

The spatial interaction relation is determined by threshold (Molchan and Dmitrieva, 1992):

$$\log d = 0.4\, M_0 - 1.943 + k, \tag{4.4}$$

where d is the distance in kilometres and k is constant which is equal to 1 for the distance to the largest earthquake and equal to 0 for the distance to the last one.

The extent of temporal interaction zone is based on Omori´s law:

$$n(t) = \frac{k}{(c+t)^p}, \tag{4.5}$$

where k and c are constants which vary between earthquake sequences and p is the constant which detemines the decay rate and typically is equal to 0.6 – 1.5.

All so linked earthquakes define a cluster. The largest earthquake in a cluster is considered to be a mainshock and smaller ones are divided into foreshocks and aftershocks.

The Reasenberg algorithm is widely used in seismic hazard analysis. The algorithm depends on several parameters. Frequently used sets of parameters for Reasenberg algorithm are presented in Tab. 2.

	Standard	**Min**	**Max**
τ_{min} **(days)**	1	0.5	2.5
τ_{max} **(days)**	10	3	15
p_1	0.95	0.9	0.99
x_k	0.5	0	1

x_{meff}	1.5	1.6	1.8
r_{fact}	10	5	20

Tab. 2: Short overview of frequently used sets of parameters for Reasenberg algorithm.

The parameters τ_{min} and τ_{max} describe the minimum and maximum look – ahead time of observing the next earthquake with a probability p_1. These three parameters are used in equation

$$\tau = -\ln(1 - p_1)\, t / 10^{2(\Delta M - 1)/3}, \tag{4.6}$$

assuming the Omori decay rate equal to 1 and $\Delta M = M_{mainshock} - x_{meff}$, where x_{meff} denotes the minimum magnitude cutoff for the earthquake catalogue. In clusters, the effective cutoff magnitude x_{meff} is raised by a factor x_k of the largest earthquake in the cluster. The parameter r_{fact} denotes the number of crack radii which surround each earthquake within which we consider linking an event into an existing cluster.

The results of the application of cluster method on the earthquake catalogue are summed up in Tab. 3.

	Reasenberg Standard	**Reasenberg Min**	**Reasenberg Max**
Foreshocks	180	138	169
Mainshocks	2655	3152	2527
Aftershocks	885	430	1024

Tab. 3: Results of the application of cluster method on the earthquake catalogue.

4.3.2 Window method

The second declustering method is based on the creation of temporal and spatial windows for foreshocks and aftershocks depending on the moment magnitude. When the earthquake „falls“ into a temporal and spatial window of another larger earthquake, it is marked as foreshock/aftershock. The biggest disadvantage of this method is that two earthquakes of the same size are always considered to be two mainshocks.

We used the following three sets of temporal and spatial windows and then we compared the results.

- Burkhard and Grünthal (2009) (4.7)

  temporal window for aftershocks (in days)

  $dT(M_W) = \exp\left(-4{,}77 + \sqrt{0{,}62 + 17{,}32M_W}\right),$ for $M_W < 7{,}8$

  $dT(M_W) = \exp(6{,}44 + 0{,}055M_W),$ for $M_W \geq 7{,}8$

  spatial window (in kilometres)

  $dR(M_W) = \exp(1{,}77 + \sqrt{0{,}037 + 1{,}02M_W}).$

- Gardener and Knopoff (1974) (4.8)

  temporal window for aftershocks (in days)

  $dT(M_W) = 10^{0{,}032M_W+2{,}7389},$ for $M_W \geq 6{,}5$

  $dT(M_W) = 10^{0{,}5409M_W-0{,}547},$ else

  spatial window (in kilometres)

  $dR(M_W) = 10^{0{,}1238M_W+0{,}983}.$

- Uhrhammer (1986) (4.9)

  temporal window for aftershocks (in days)

  $dT(M_W) = e^{-2{,}87+1{,}235M_W},$

  spatial window (in kilometres)

  $dR(M_W) = e^{-1{,}024+0{,}804M_W}.$

The results of the application of the window method on the earthquake catalogue are summed up in Tab. 4.

	Burkhard and Grünthal (2009)	**Gardener and Knopoff (1974)**	**Uhrhammer (1986)**
Foreshocks	297	305	211
Mainshocks	1957	2118	2624
Aftershocks	1466	1297	885

Tab. 4: Results of the application of window method on the earthquake catalogue.

4.3.3 Test of application of Poissonian distribution

We should be in an ideal case able to describe the mainshocks as a Poissonian process. Therefore we divided the time period from 1950 to 2011 into 100-days long time windows and checked the count of earthquakes with macroseismic intensity III and higher in every time window. In a histrogram we graphically depict the number of windows with 0, 1, 2, etc. earthquakes. We computed the mean value of earthquakes in a time window and then computed Poissonian fit for our data. Then we used the chi-square – „goodness of fit“ test.

The principle of chi-square test is the comparison between real data and theoretical data:

$$X^2 = \sum_{i=1}^{k} \frac{(x_{real} - x_{theor})^2}{x_{theor}}. \quad (4.10)$$

The result of the chi-square test is then compared with the selected significance level (probability to reject the true hypothesis). If the computed value is smaller than the value for significance level, the hypothesis is accepted, the data do not contradict the Poissonian hypothesis.

The graphical comparisons for all considered windows between the real data and theoretical Poissonian fits are presented in Fig. 11 – Fig. 14 and the results of chi-square tests are summed up in Tab. 5.

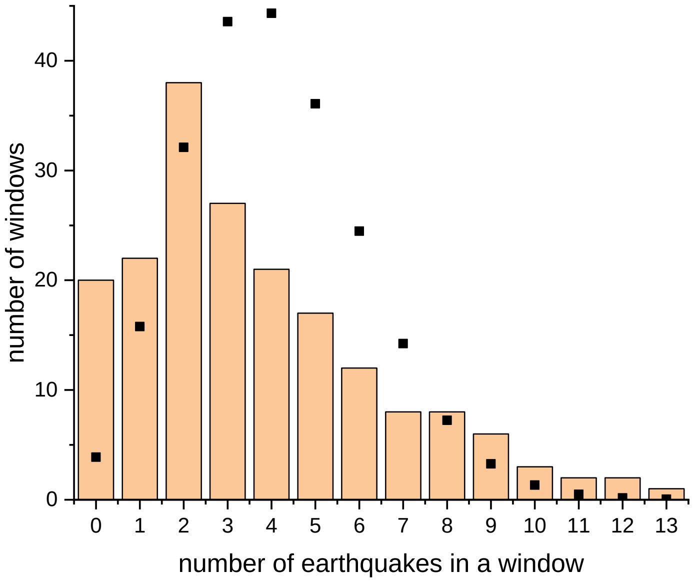

Fig. 11: Comparison of real data and theoretical Poissonian fit for earthquake catalogue declusterized by Reasenberg method with Standard parameters.

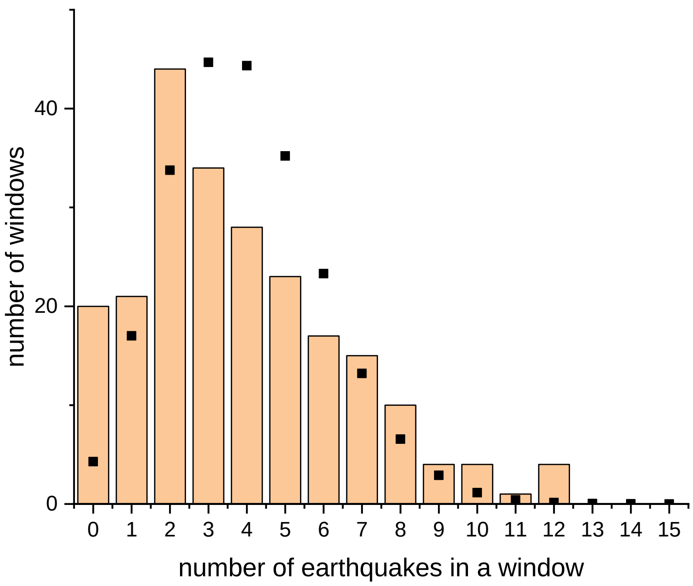

Fig. 12: Comparison of real data and theoretical Poissonian fit for earthquake catalogue declusterized by window method with parameters Uhrhammer (1986).

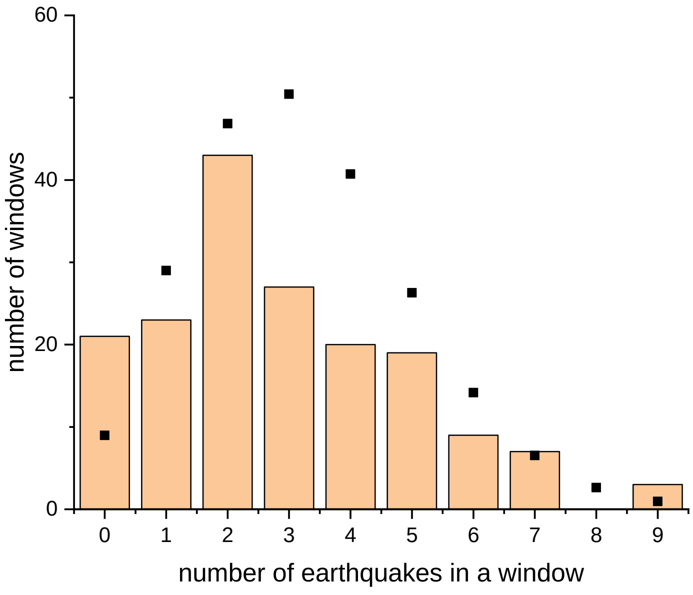

Fig. 13: Comparison of real data and theoretical Poissonian fit for earthquake catalogue declusterized by window method with parameters Gardener and Knopoff (1974).

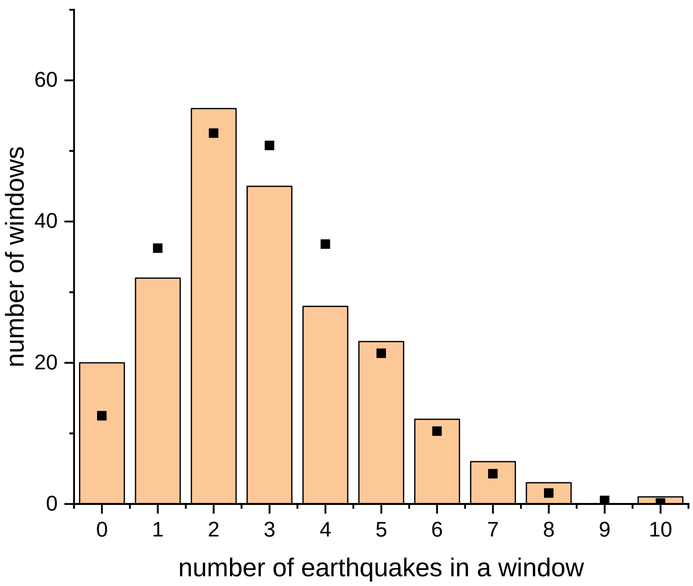

Fig. 14: Comparison of real data and theoretical Poissonian fit for earthquake catalogue declusterized by window method with parameters Burkhard and Grünthal (2009).

	Reasenberg Standard	Burkhard and Grünthal (2009)	Gardener and Knopoff (1974)	Uhrhammer (1986)
Chi-square value	122.58	10.33	43.12	97.05
Threshold value	$X^2_{0.1}(10) = 15.99$ $X^2_{0.01}(10) = 23.21$	$X^2_{0.1}(6) = 10.64$ $X^2_{0.01}(6) = 16.81$	$X^2_{0.1}(9) = 14.68$ $X^2_{0.01}(9) = 21.67$	$X^2_{0.1}(10) = 15.99$ $X^2_{0.01}(10) = 23.21$

Tab. 5: Results of chi-square test.

As we can see, only one window method gives results, which can be described as a Poissonian process – Burkhard and Grünthal (2009). Therefore we decided to use the catalogue declusterized by Burkhard and Grünthal (2009) window parameters in further computations.

4.4 Completeness analysis of the catalogue

The completeness of the catalogue in time was determined by two methods – cumulative visual method (Tinti and Mulargia, 1985) and Stepp method (Stepp, 1972) and we compared the results.

4.4.1 Cumulative visual method

We divided earthquakes from the catalogue declusterized by window method into 9 intensity classes – III and less, III – IV, IV, IV – V, V, V – VI, VI, VI – VII, VII and more, and created graphical dependence of cumulative number of earthquakes from given intensity class on time. The last linear section of curve indicates the stable seismic activity i.e. the lower boundary of the time period in which we consider the catalogue to be complete. The results of cumulative visual method for mainshocks obtained by Burkhard and Grünthal (2009) are presented in Fig. 15 and Fig. 16.

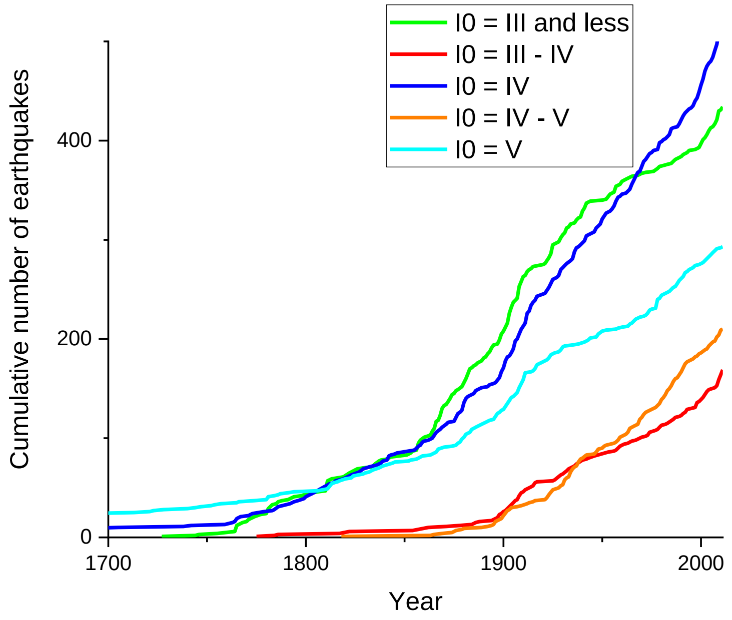

Fig. 15: Results of cumulative visual method for intensity classes III and less to V.

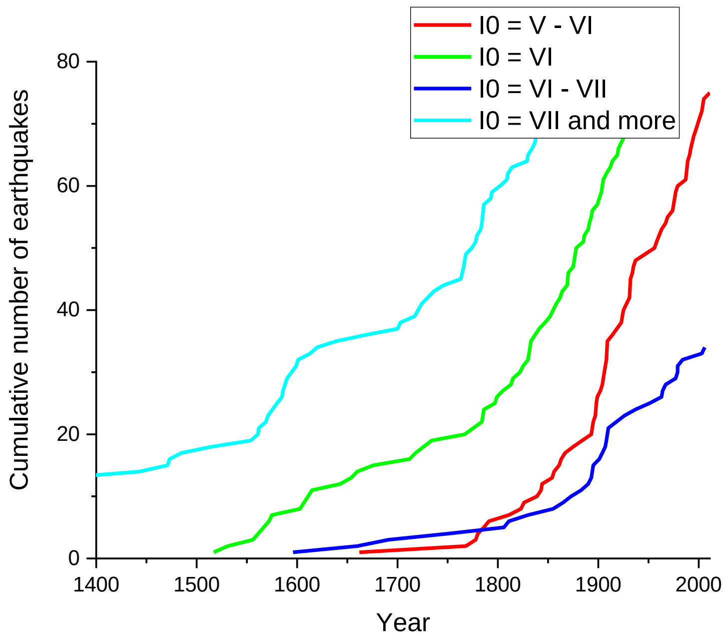

Fig. 16: Results of cumulative visual method for intensity classes V – VI to VII and more.

4.4.2 Stepp method

The Stepp method (Stepp, 1972) is a widely used statistical procedure for assessment of completeness time of the reported magnitudes or intensities. We assume that earthqake sequences can be modelled as a Poissonian distribution. The earthquakes in the catalogue are divided into different intensity classes and each intensity is modeled as a point process in time. For each intensity class, mean rate of occurrence of the earthquake is determined.

The estimate of mean rate per unit time interval of the sample is

$$\lambda = \left(\frac{1}{n}\right) \sum_{i=1}^{n} k_i, \tag{4.7}$$

where k_1, k_2, ..., k_n is the number of earthquakes per unit time interval and n is the number of unit time intervals.

The variance of the estimate of mean rate λ is

$$\sigma_\lambda^2 = \frac{\lambda}{n}. \tag{4.8}$$

If we consider the unit time interval to be one year, we get

$$\sigma_\lambda = \sqrt{\frac{\lambda}{T}} \tag{4.9}$$

as the standard deviation of the estimate of the mean rate, where T is the duration of the interval. Therefore if the earthquake data series is stationary (the case of complete catalogue), λ is constant and σ_λ varies as $1/\sqrt{T}$. Standard deviation of the mean rate estimate as a function of sample length is then plotted along with tangent lines with slope $1/\sqrt{T}$ and the deviation of the mean rate estimate from the tangent line indicates the time period in which we consider the catalogue to be complete. The results of Stepp method for the mainshocks and the same intensity classes as in 4.4.1 are presented in Fig. 17 – Fig. 19. The completeness periods determined by both methods are summed up in Tab. 5.

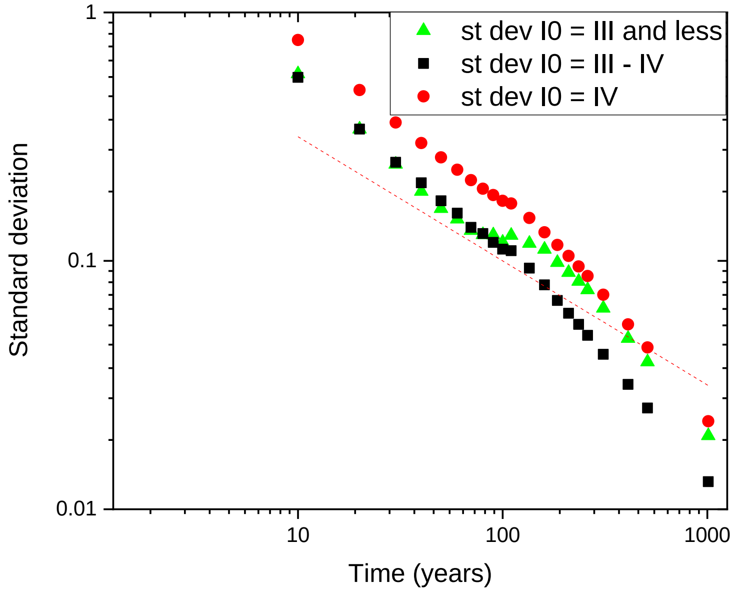

Fig. 17: Results of Stepp method for intensity classes III to IV.

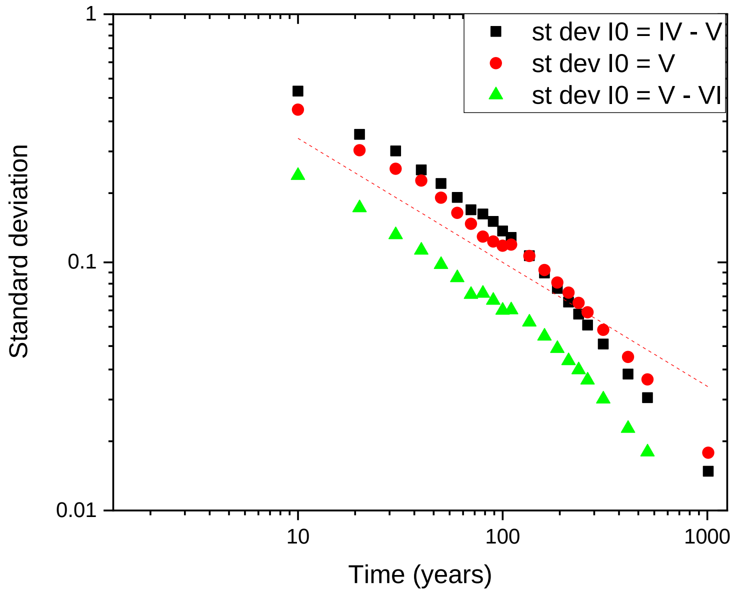

Fig. 18: Results of Stepp method for intensity classes IV-V to V-VI.

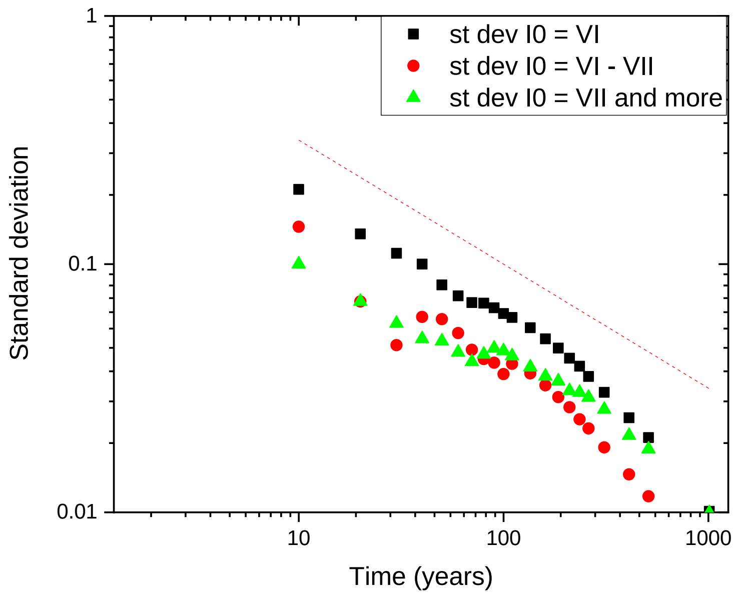

Fig. 19: Results of Stepp method for intensity classes VI to VII and more.

Intensity class	Stepp method		Cumulative visual method		Number of earthquakes
	Years of completeness	Number of earthquakes	Years of completeness	Number of earthquakes	
III and less	100	307	80	238	695
III – IV	110	207	110	207	236
IV	110	482	110	482	725
IV – V	110	244	110	244	272
V	135	249	160	272	372
V – VI	135	67	160	73	90
VI	235	98	220	91	122
VI – VII	160	28	180	30	36
VII and more	310	67	310	67	107

Tab. 5: Periods of completeness obtained by cumulative visual method and Stepp method.

5 Selection of IPEs

For the seismic hazard analysis in terms of macroseismic intensity, it is very important to properly select suitable IPEs for further computations. We considered two types of IPEs – the equations depending on epicentral intensity and the equations depending on moment magnitude. We considered 2 IPEs depending on epicentral intensity and 11 IPEs depending on moment magnitude. IPEs differ in some physical aspects such as magnitude range, distance range and intensity scale type. Although we know that the same intensity degrees from different intensity scales are not equal, we considered them to be equal to simplify the computations. Two IPEs with macroseismic intensity depending on epicentral intensity are Labák (2000) and Stromeyer and Grünthal (2009). Labák (2000) presents two types of IPEs – the equation where macroseismic intensity directly depends on epicentral intensity and the equation where macroseismic intensity represents the difference between epicentral and site intensity.

The functional forms of the IPEs Labák (2000) are shown in (5.1) and (5.2). The functional form of the IPE Stromeyer and Grünthal (2009) is presented in (5.3).

$$I - I_0 = 0.435 - 1.231 \log R - 0.019R, \tag{5.1}$$

$$I = 1.637 - 1.183 \log R - 0.015R + 0.783I_0, \tag{5.2}$$

$$dI = I - I_0 = 2.8 \log\left(\sqrt{\frac{R^2+h^2}{h^2}}\right) + 0.0013\left(\sqrt{R^2 + h^2} - h\right), \tag{5.3}$$

where I is the site intensity, I_0 is the epicentral intensity, R is the epicentral distance and h is the focal depth. The graphical dependence of the site intensity with fixed values of epicentral intensity (degrees III / V / VIII) on the distance for three presented equations is shown in Fig. 20.

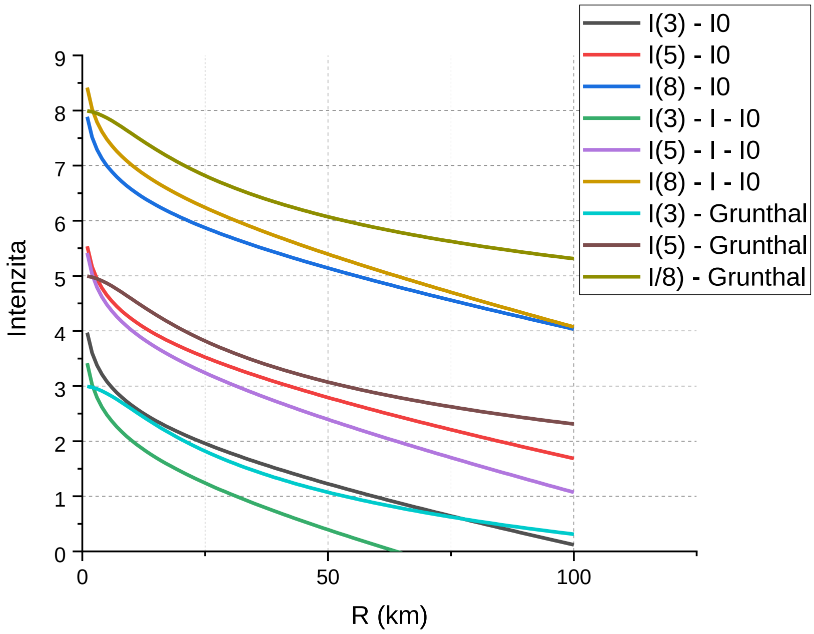

Fig. 20: The graphical dependence of site intensity on the epicentral distance with fixed epicentral intensities for IPEs (5.1), (5.2) and (5.3) .

The second considered type of IPEs are the equations with the site intensity depending on moment magnitude. We compared 11 different available equations (Cua et al., 2010) and selected three of them for further computations.

Quick overview of all considered IPEs with macroseismic intensity depending on moment magnitude is presented in Tab. 6. The functional forms of all presented equations are outlined below the table.

Reference	**Intensity scale**	**Intensity range**	**Distance range (km)**	**Type of distance**	**Magnitude range**	**Region**
Atkinson and Wald (2007)	MMI	2-10	2-500	R_{rup}	2.3-7.8	California, USA

Atkinson and Wald (2007)	MMI	2-11	6-1000	R_{rup}	2.0-7.8	Eastern North America
Bakun and Scotti (2006)	MSK	3-7	<150	R_{epi}	4.9-6.0	French SCR
Bakun and Scotti (2006)	MSK	3-7	<150	R_{epi}	4.9-6.0	Southern France
Bakun (2006)	MMI	3-8	<500	R_{epi}	4.6-7.3	Basin and Range, USA
Bakun and Wentworth (1997)	MMI	3-9	<500	R_{epi}	4.4-6.9	California, USA
Bakun et al. (2003)	MMI	3-7	<1200	R_{epi}	3.7-7.3	Eastern North America
Chandler and Lam (2002)	MMI	4-10	<300	R_{epi}	3.3-8.0	South China
Dowrick and Rhoades (2005)	MMI	3-11	<500	R_{rup}	4.6-8.2	New Zealand – Main Region
Dowrick and Rhoades (2005)	MMI	3-11	<500	R_{rup}	5.2-7.3	New Zealand – Deep Region
Pasolini et al. (2008)	MCS	4-11	1-200	R_{epi}	4.4-7.4	Italy

Tab. 6: Overview of all considered IPEs and their physical characteristics.

It is important to note that different types of IPEs may use different types of distances, which are not interchangeable. Three most commonly used types are R_{rup} (closest distance from the site to the rupture), R_{epi} (epicentral distance) and R_{JB} (Joyner-Boore distance – the closest horizontal distance between the site and vertical projection of the rupture). As we can see, the considered types of IPEs use only R_{epi} and R_{rup}. The graphical description of various types of distances is presented in Fig. 21.

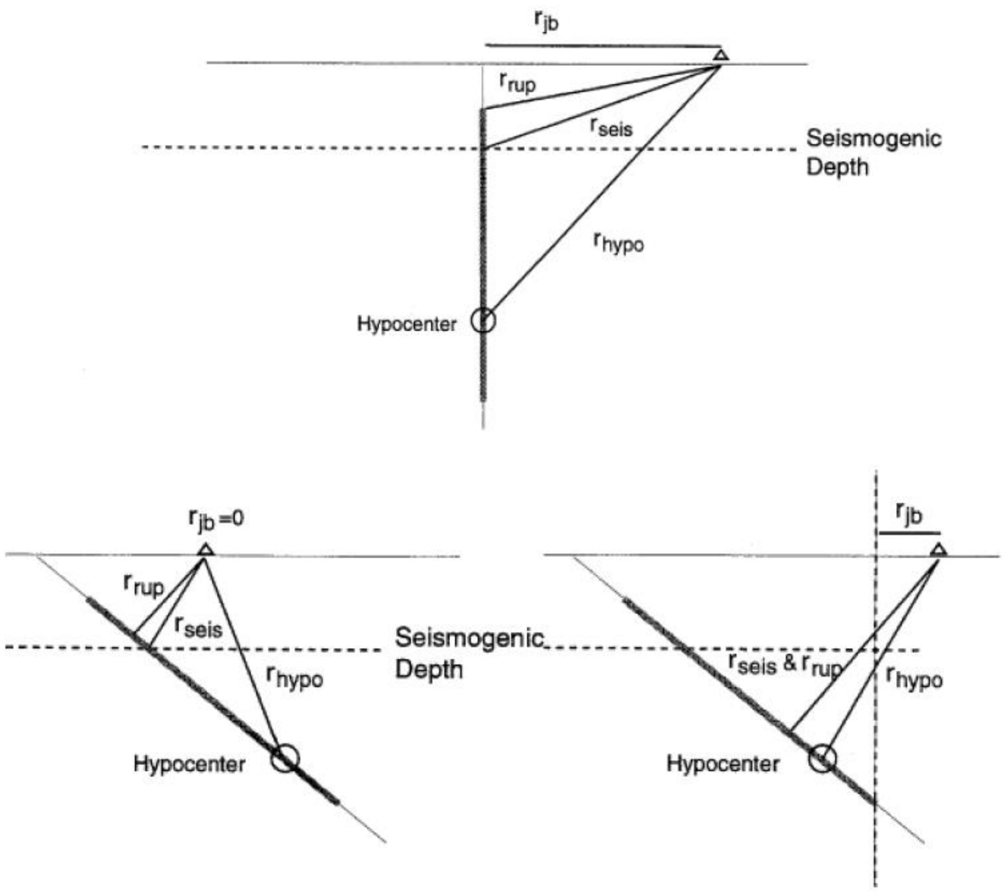

Fig. 21: Types of distances for different types of orientation of the fault (source: Abrahamson and Shedlock, 1997).

Atkinson and Wald (2007), California, USA

$$I_{MMI} = 12{,}27 + 2{,}270(M_W - 6) + 0{,}1204(M_W - 6)^2 - 1{,}30 \log R - 0{,}0007070R + 1{,}95B - 0{,}577 M_W \log R, \quad (5.1)$$

where $R = \sqrt{{R_{rup}}^2 + h^2}$

$h = 14$

$B = 0$ for $R \leq 30$; $\log R/30$ for $R > 30$

$\sigma \approx 0{,}4$

Atkinson and Wald (2007), Eastern North America

$$I_{MMI} = 11{,}72 + 2{,}36(M_W - 6) + 0{,}1155(M_W - 6)^2 - 0{,}44 \log R - 0{,}002044R + 2{,}31B - 0{,}479 M_W \log R, \quad (5.2)$$

where $R = \sqrt{{R_{rup}}^2 + h^2}$

$h = 17$

$B = 0$ for $R \leq 80$; $\log R/80$ for $R > 80$

$\sigma \approx 0{,}4$

Bakun and Scotti (2006), French SCR

$$I_{MSK} = 4{,}48 + 1{,}27M_W - 3{,}37\log(\sqrt{{R_{epi}}^2 + h^2}), \quad (5.3)$$

Bakun and Scotti (2006), Southern France

$$I_{MSK} = 4{,}66 + 1{,}27M_W - 3{,}83\log(\sqrt{{R_{epi}}^2 + h^2}), \quad (5.4)$$

Bakun (2006), Basin and Range, USA

$$I_{MMI} = 0{,}44 + 1{,}7M_W - 0{,}0048\Delta_h - 2{,}73\log(\Delta_h), \quad (5.5)$$

where $\Delta_h = \sqrt{{R_{epi}}^2 + h^2}$

$h = 10$

$\sigma = 0{,}58$

Bakun and Wentworth (1997), California, USA

$$I_{MMI} = 3{,}67 + 1{,}17M_W - 3{,}19\log(R_{epi}), \quad (5.6)$$

Bakun et al. (2003). Eastern North America

$$I_{MMI} = 1{,}41 + 1{,}68M_W - 0{,}00345R_{epi} - 2{,}08\log(R_{epi}), \quad (5.7)$$

Chandler and Lam (2002), South China

$$I_{MMI} = -0{,}8919 + 1{,}4798M_W - 0{,}1311\ln\left[\frac{R_{epi}+R_0}{R_0}\right] - 0{,}0364\,R_{epi}, \quad (5.8)$$

for $R_{epi} \leq 45km$

$I_{MMI} = -0{,}8919 + 1{,}4798M_W - 0{,}1311 \ln\left[\frac{R_{epi}+R_0}{R_0}\right] - 0{,}0364\, R_{epi} +$

$0{,}0193(R_{epi} - 45)$

for $45 < R_{epi} \le 75\ km$

$I_{MMI} = -0{,}8919 + 1{,}4798M_W - 0{,}1311 \ln\left[\frac{R_{epi}+R_0}{R_0}\right] - 0{,}0364\, R_{epi} +$

$0{,}0193(R_{epi} - 45) + 0{,}0085(R_{epi} - 75)$

for $R_{epi} > 75\ km$

where $R_0 = \left(\frac{1}{2}\right) \mathrm{x}10^{(0{,}74M_W - 3{,}55)}$

$\sigma \approx 0{,}7$

Dowrick and Rhoades (2005), New Zealand, Main Region

$$I_{MMI} = 4{,}4 + 1{,}26M_W - 3{,}67 \log(r^3 + d^3)^{\frac{1}{3}} + 0{,}012h + 0{,}409\delta_c, \quad (5.9)$$

where $\delta_c = 1$ for crustal events / 0 for all other events

$d = 11{,}78$

$r \approx R_{rup}$

$\sigma = 0{,}43$

Dowrick and Rhoades (2005), New Zealand, Deep Region

$$I_{MMI} = 3{,}76 + 1{,}48M_W - 3{,}5 \log r + 0{,}0031h, \quad (5.10)$$

where $r \approx R_{rup}$

$\sigma = 0{,}42$

Pasolini et al. (2008), Italy

$$I_{MCS} = I_E - 0{,}0086\left(\sqrt{R_{epi}{}^2 + h^2} - h\right) - 1{,}037\left(\ln\left(\sqrt{R_{epi}{}^2 + h^2}\right) - \ln(h)\right), \quad (5.11)$$

where $I_E = 2{,}46M_W - 5{,}862$

$h = 3{,}91$

$\sigma = 0{,}69$

To compare the results we divided equations into two classes – those depending on R_{rup} and those depending on R_{epi} and plotted the dependance of macroseismic intensity on the distance for fixed moment magnitude $M_W = 6$. For equations without fixed value of h, we considered h =12 km. The graphical depictions of computed macroseismic intensity for both classes of IPEs are presented in Fig. 22 and Fig. 23. For further computations we selected IPEs Bakun (2006), Bakun and Scotti (2006) and Pasolini et al. (2008). The selection is based on the fact, that the attenuation of macroseismic intensity in the Western Carpathians is similar to the attenuation of macroseismic intensity in the region of California (Labák, 2000). Moreover, the three selected IPEs use three different intensity scales (MMI, MSK, MCS).

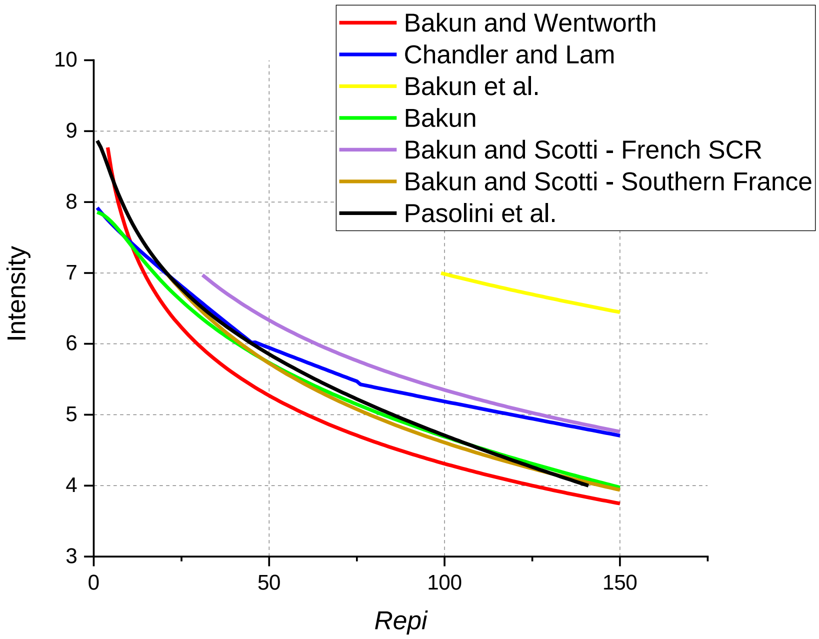

Fig. 22: Dependence of computed macroseismic intensity on epicentral intensity for various IPEs.

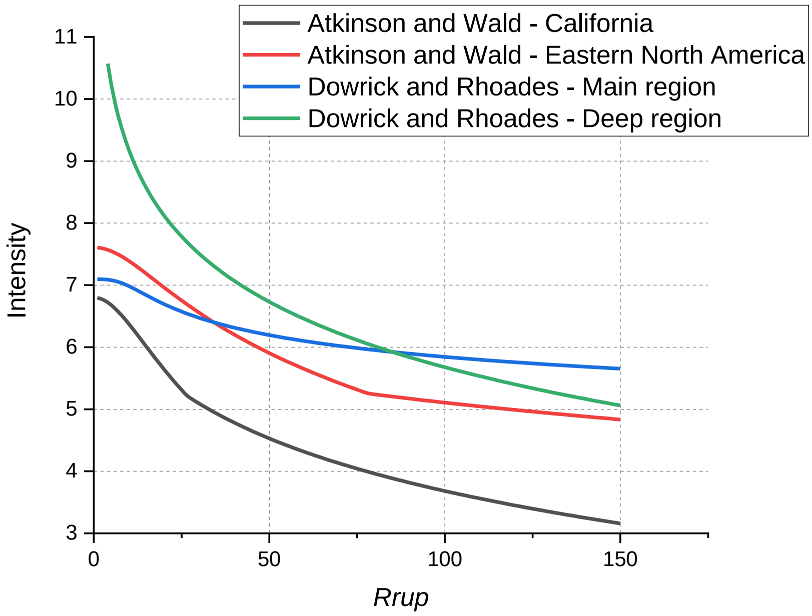

Fig. 23: Dependence of computed macroseismic intensity on the closest distance to the rupture for various IPEs.

6 Seismotectonic model

Seismotectonic model for the Slovak territory abbreviated as SK2011 (Hók et al., 2016), was created from the seismotectonic model of the project SESAME (Fig. 23) and from seismological, geological and geophysical database for Slovakia. Seismic source zones are the discrete parts of the area of interest, where we consider the seismic activity to be similar or to have similar behaviour.

Seismic source zones are covering the whole area of Slovakia and also small parts of neighbouring countries. For each seismic source zone we determined the maximum potential intensity, Gutenberg-Richter parameters a and b (1.11) and also the seismic activity rate λ by using cumulative least square method.

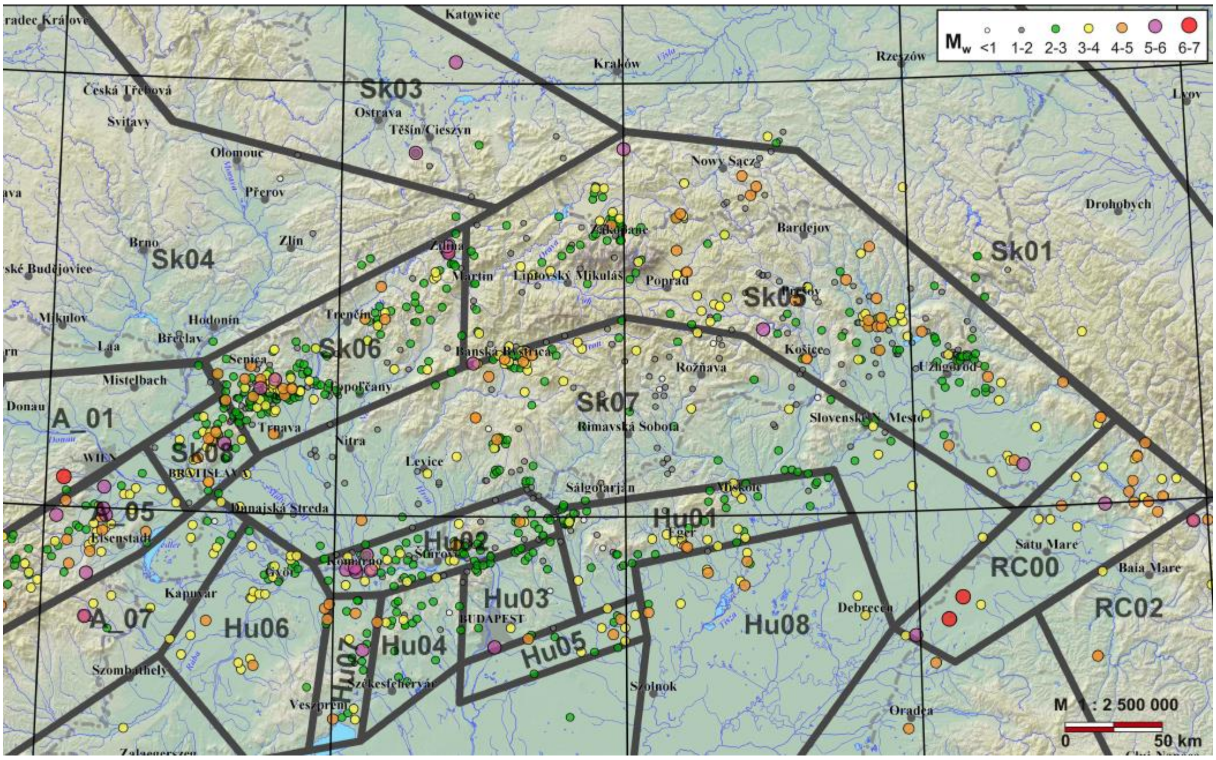

Fig. 23: The division of the area of Slovakia into seismic source zones as presented in project SESAME with epicenters from earthquake catalogue GPI SAS (2012).

The seismic source zones in model SK2011 can be divided into four groups

1. Alcapa domain – Western Carpathians, Eastern Austria and Northern Hungary. Denoted as SK1 – SK7.

2. North-Pannonian domain – mostly the area of Hungary. Denoted as H1 – H8.

3. Alcapa domain – Eastern Alps, Eastern Austria and South-East Austria. Denoted as A1, A5 and A7.

4. Consolidated European platform – mostly the area of Czech Republic and Poland. Denoted as P1 – P3.

The division of the area of Slovakia into seismic source zones as presented in seismotectonic model SK2011 with graphical denotion of epicenters of all earthquakes from earthquake catalogue GPI SAS (2012) is shown in Fig. 24. The depth of all presented seismic source zones is 12 km.

For the computation of the seismic hazard map of the Slovak territory, we used both presented seismotectonic models SK2011 and SESAME.

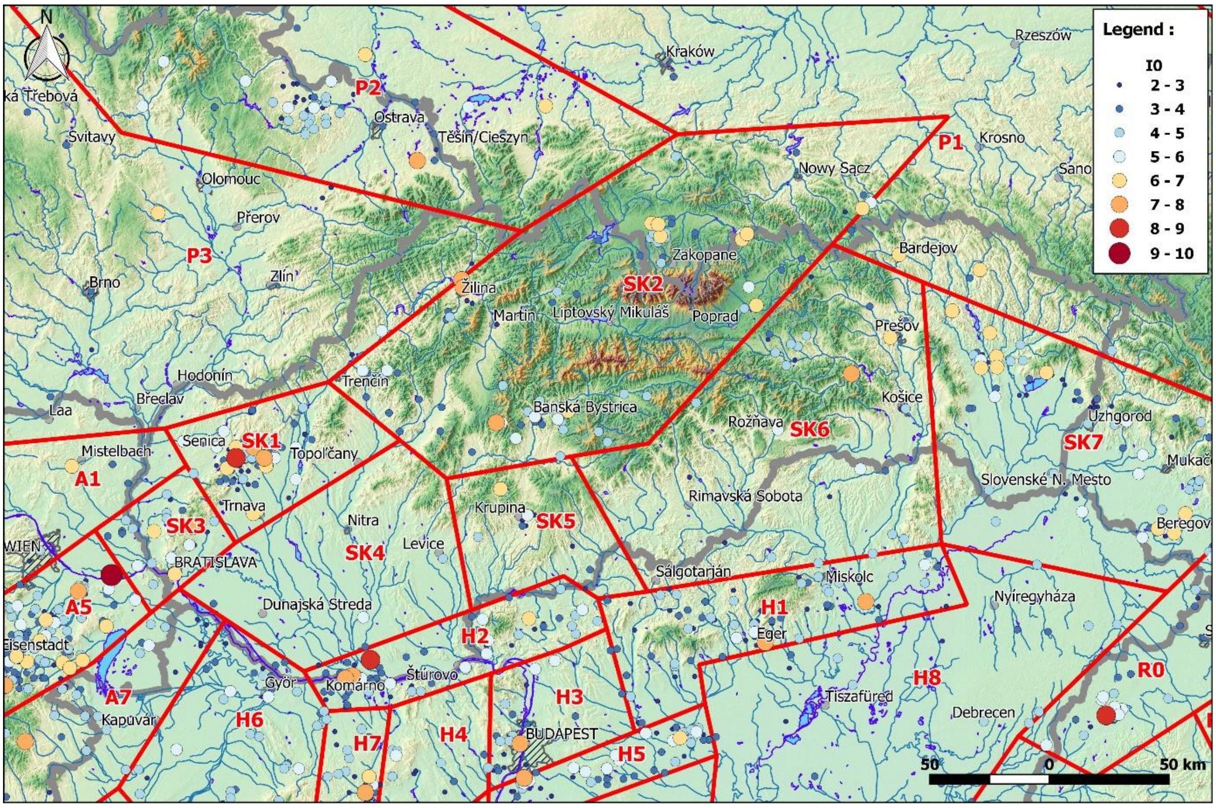

Fig. 24: The division of the area of Slovakia into seismic source zones as presented in seismotectonic model SK2011 with epicenters from earthquake catalogue GPI SAS (2012).

7 Maximum potential intensity and seismic source parameters

For every seismic source zone, we denoted the maximum potential intensity as the macroseismic intensity of the strongest observed earthquake plus half-intensity degree. From all mainshocks with epicenters in a particular seismic source zone we denoted by cumulative least squares method the Gutenberg-Richter parameters a,b (and therefore β) and seismic activity rate λ. The seismic activity rate was computed for the intensity degree III and then recomputed for intensity degree V by (7.1).

$$\lambda_V = \lambda_{III}\left(1 - \frac{1-e^{-\beta(5-3)}}{1-e^{-\beta(I^{max}-3)}}\right), \tag{7.1}$$

where λ_V is the seismic activity rate for the intensity degree V, λ_{III} is the seismic activity rate for the intensity degree III, β is the Gutenberg-Richter parameter and I^{max} is the macroseismic intensity of the largest observed earthquake in the seismic source zone.

The parameters for all seismic source zones of seismotectonic model SK2011 are presented in Tab. 7.

Seismic source zone	Maximum potential intensity	***a***	***b***	***β***	***λ(5)***
SK1	9	1.7322	-0.5314	-1.2235	0.1334
SK2	8.5	1.1602	-0.4084	-0.9403	0.1209
SK3	8	1.0892	-0.5109	-1.1765	0.0403
SK4	6.5	-0.2319	-0.3629	-0.8357	0.0068
SK5	7	0.2501	-0.3749	-0.8631	0.0202
SK6	8.5	-0.0961	-0.3446	-0.7934	0.0183
SK7	7.5	1.1848	-0.3963	-0.9126	0.1457
H1	8.5	2.4434	-0.7474	-1.7209	0.0640
H2	9	1.3870	-0.5061	-1.1655	0.0883
H3	8.5	1.0572	-0.5743	-1.3224	0.0152
H4	6.5	0.4452	-0.4514	-1.0395	0.0125
H5	8	2.5315	-0.7179	-1.6530	0.1094
H6	6	1.0337	-0.4406	-1.0146	0.0453
H7	8.5	1.8897	-0.5540	-1.2756	0.1346
H8	5.5	0.6672	-0.4291	-0.9881	0.0142
A1	9.5	0.5246	-0.3927	-0.9042	0.0359
A5	10	2.5302	-0.5077	-1.1690	0.8003
A7	9.5	2.0143	-0.6116	-1.4081	0.0748
P1	7.5	0.3618	-0.3470	-0.7989	0.0376
P2	8	0.9761	-0.4020	-0.9257	0.0866
P3	8.5	1.2316	-0.4831	-1.1124	0.0643

Tab. 7: Results of the parameters a,b,β and λ and maximum potential intensity for all seismic source zones of seismotectonic model SK2011.

8 Probabilistic seismic hazard analysis of the Slovak territory in terms of macroseismic intensity

The probabilistic seismic hazard assessment of Slovak territory in terms of macroseismic intensity was realized by computer programme CRISIS2007 ver. 7.6 (Ordaz et al., 2007). The seismic source zones were considered to be areal zones with constant depth of 12 km. The boundaries of the zones are linear and the longitudes and latitudes of the boundary points are from Kysel (2014).

We considered the parameters K_1 and K_2 from formula for computation of the rupture radius used by the software to be equal $K_1 = 0.1015$ and $K_2 = 0$. This means that the rupture cannot propagate outside the seismic source zone. CRISIS2007 characterizes the seismicity of source zones by Gutenberg-Richter parameters, their uncertainties, minimum considered intensity and maximum potential intensity for every seismic source zone. We used the values from Tab. 7.

We chose the minimum considered intensity to be of degree V. This value is the lowest intensity degree that causes damages of the buildings.

The computational area is characterized by longitude and latitude of the left lowermost point, the length of the incremental step in west-east and north-south direction and the number of steps in both directions. The information about the area of the interest is summed up in Tab. 8.

	Longitude	**Latitude**
Position of lowermost left point	16.500	47.400
Size of the step (degree)	0.025	0.025
Number of steps	264	108

Tab. 8: The parameters of the area of interest.

We computed the seismic hazard map for various sets of input parameters. Firstly, we used two IPEs with site intensity depending on epicentral intensity - Stromeyer and Grünthal (2009) and Labák (2000). The default minimum distance of attenuation relation was set to 1 km, but this value uncovered the fact that the IPE Labák (2000) gives for small distances higher values of site intensity than the values of epicentral intensity. Therefore we alternatively tried distances 5 km and 3 km. The distance of 3 km gives the best results, therefore we decided to use this value as default minimum distance of attenuation relation. Maximum integrating distance was set to be 100 km. We tried alternative value of 150 km, but the change in maximum integrating distance cause only negligible change in values of seismic hazard, therefore we decided to use the distance of 100 km as the default value.

The second parameter we changed is the value of truncation of distribution of residues (ε). We tried the untruncated distribution and also different values of truncation ($\varepsilon = 0$, $\varepsilon = 1$, $\varepsilon = 3$) and we compared the results. The standardly used value is ε = 3 (comprise approximately 99,7% of the strong motion data), therefore we decided to use this value as the default value.

We used the seismotectonic model SK2011 as the main seismotectonic model for our computations, but we also used seismotectonic model SESAME for comparison of results.

Then we also computed the seismic hazard using the three selected IPEs with site intensity depending on moment magnitude - Bakun (2006), Bakun and Scotti (1997) and Pasolini (2008).

The return periods of the computation are 475 and 10 000 years. 475 years is one of the most commonly used return periods in seismic hazard analysis, because it equals 10% probability of exceedance in 50 years. The return period of 10 000 years was also used, because the highest values of macroseismic intensity in map with a 10 000 years return period should approximately match the highest observed/possible intensities of the area of interest, therefore it can be used as a sanity check of our hazard computation.

8.1 Seismic hazard maps using seismotectonic model SK2011 and IPEs depending on epicentral intensity

The seismic hazard maps for seismotectonic model SK2011, return periods 475 and 10 000 years, minimum distance of attenuation relation 3 km, ε = 3 and for IPEs with site intensity depending on epicentral intensity are presented in Fig. 25 - Fig 28.

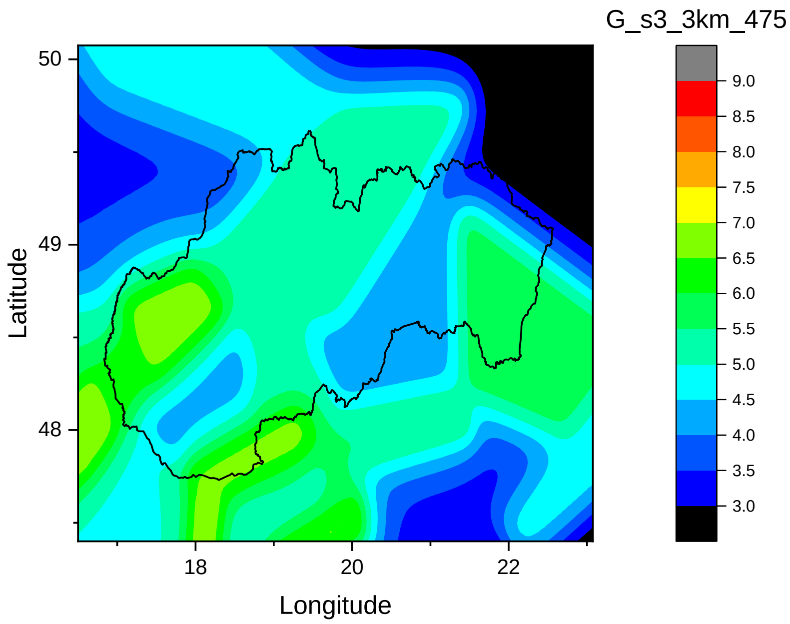

Fig. 25: Seismic hazard map computed by IPE Stromeyer and Grünthal (2009) with the minimum distance of attenuation relation 3 km, ε = 3 and for return period of 475 years.

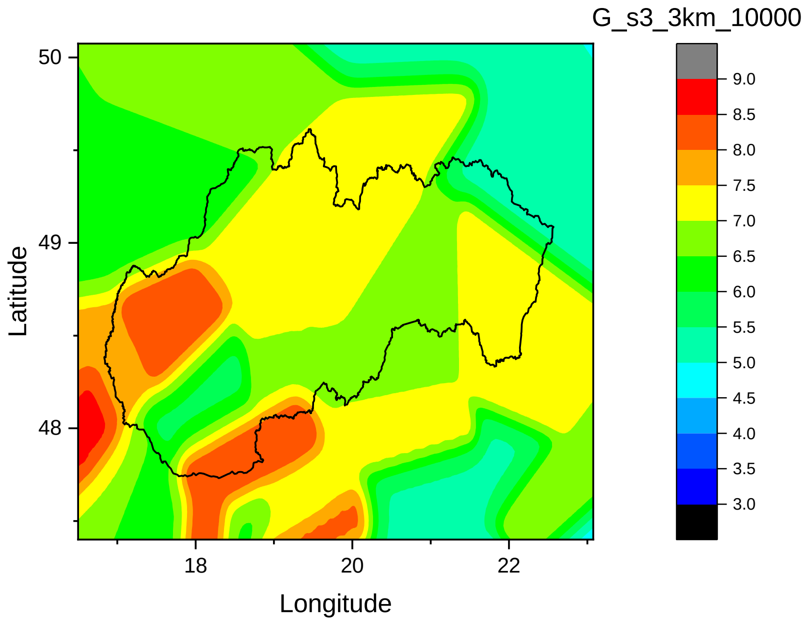

Fig. 26: Seismic hazard map computed by IPE Stromeyer and Grünthal (2009) with the minimum distance of attenuation relation 3 km, ε = 3 and for return period of 10 000 years.

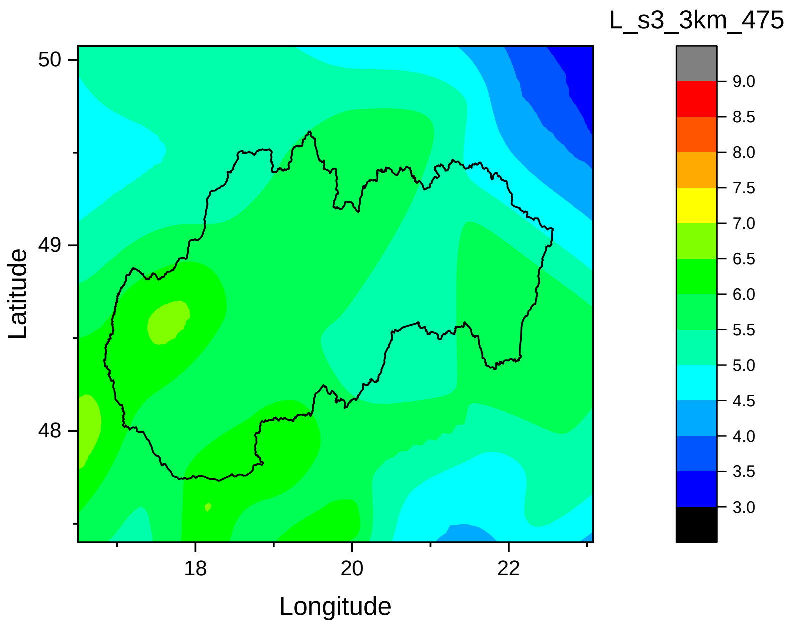

Fig. 27: Seismic hazard map computed by IPE Labák (2000) with the minimum distance of attenuation relation 3 km, ε = 3 and for return period of 475 years.

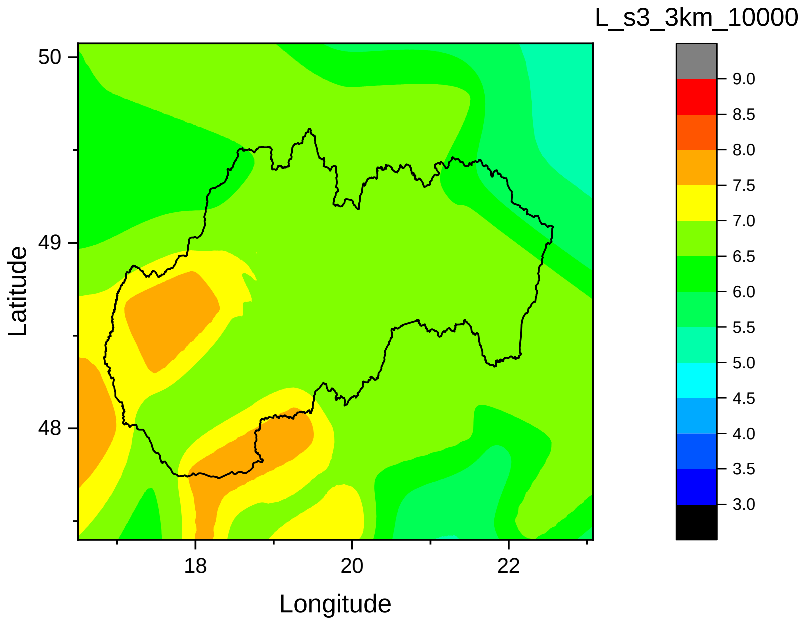

Fig. 28: Seismic hazard map computed by IPE Labák (2000) with the minimum distance of attenuation relation 3 km, ε = 3 and for return period of 10 000 years.

As we can see, both presented IPEs give similar values. The IPE Stromeyer and Grünthal (2009) gives smaller values of macroseismic intensity than IPE Labák (2000) for return period 475 years and higher values than Labák (2000) for return period 10 000 years. In Fig. 28, we can see strange structure near the area of Trnava. The reason behind this structure is unknown and we presume that it is a numerical artefact of the computation.

The seismic hazard maps for seismotectonic model SK2011, return periods 475 and 10 000 years, minimum distance of attenuation relation 1 km, ε = 3 and for IPEs with site intensity depending on epicentral intensity are presented in Fig. 29 - Fig 32.

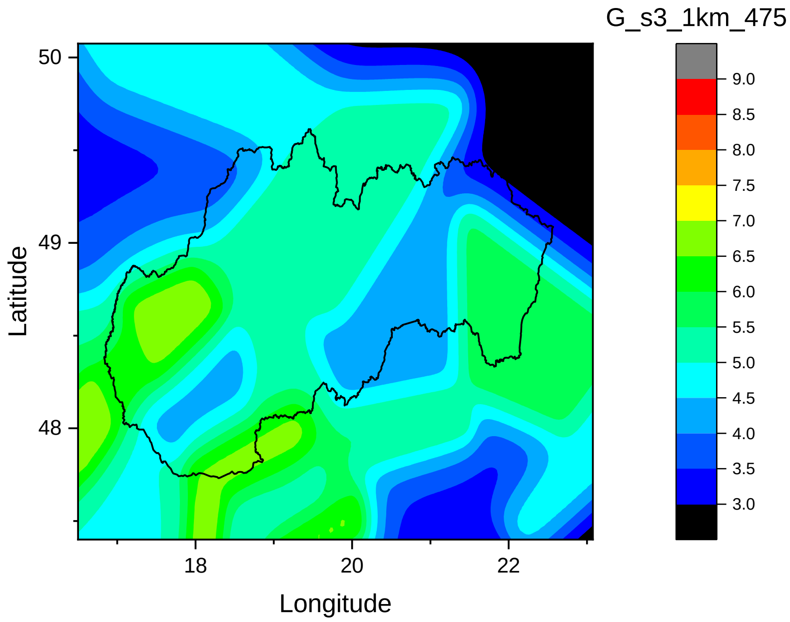

Fig. 29: Seismic hazard map computed by IPE Stromeyer and Grünthal (2009) with the minimum distance of attenuation relation 1 km, σ = 3 and for return period of 475 years.

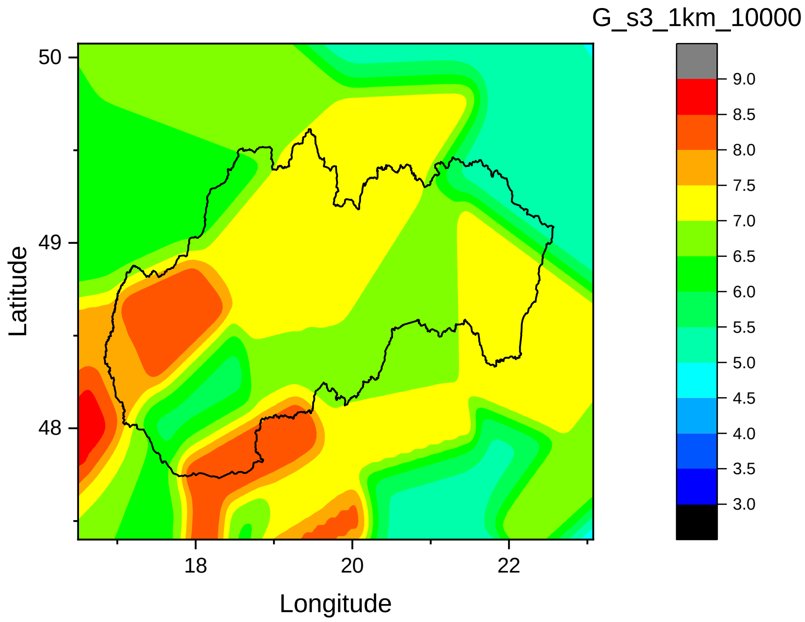

Fig. 30: Seismic hazard map computed by IPE Stromeyer and Grünthal (2009) with the minimum distance of attenuation relation 1 km, σ = 3 and for return period of 10 000 years.

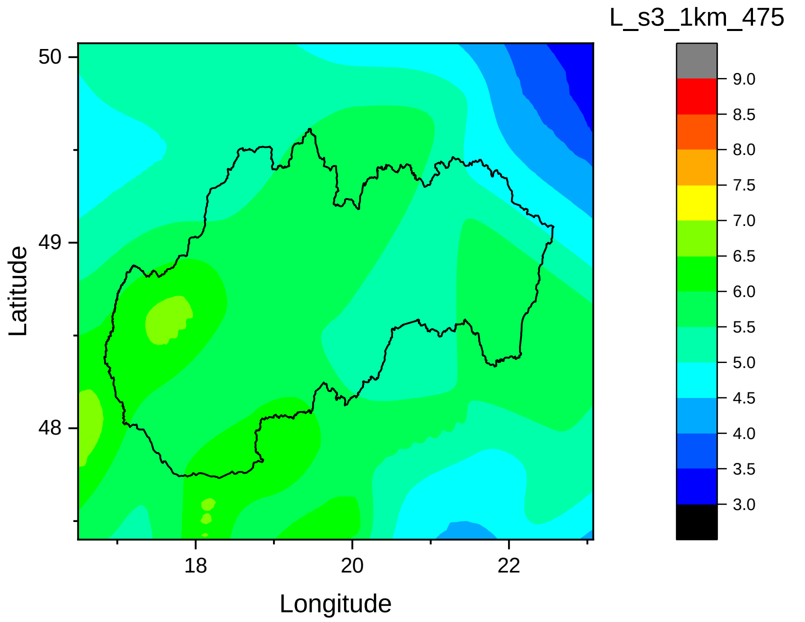

Fig. 31: Seismic hazard map computed by IPE Labák (2000) with the minimum distance of attenuation relation 1 km, σ = 3 and for return period of 475 years.

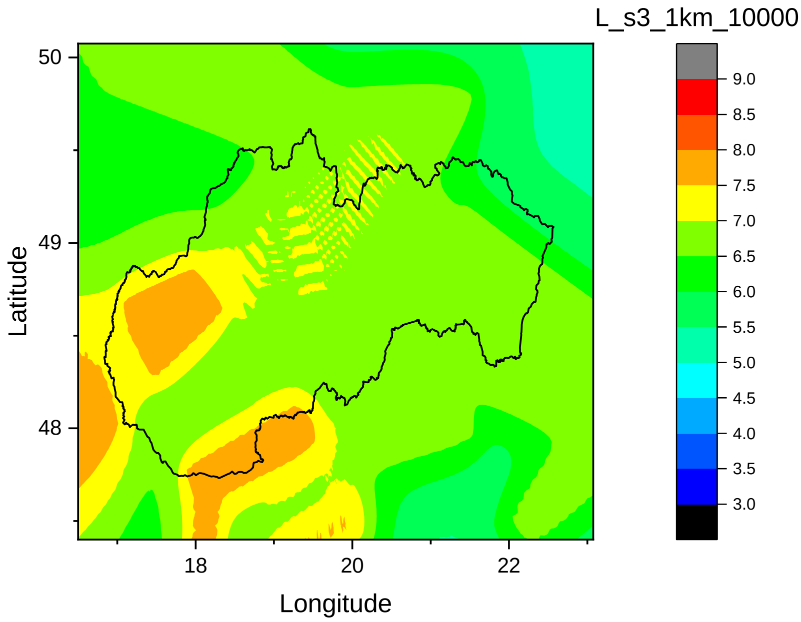

Fig. 32: Seismic hazard map computed by IPE Labák (2000) with the minimum distance of attenuation relation 1 km, σ = 3 and for return period of 10 000 years.

As we can see, this change of the parameter has only small effect on the resulting values of macroseismic intensity. However, IPE Labák (2000) saturates for small distances and that fact results in zig-zag borders and blurred point-like structures in Fig. 32.

8.2 Effect of sigma truncation

To show the effect of truncation of distribution of ground-motion residuals on seismic hazard, we changed the value of ε, that is the number of standard deviation, to $\varepsilon = 0$ (mean hazard), $\varepsilon = 1$. We also performed the computation for untruncated distribution. We notice that the results for $\varepsilon = 3$ are presented in the previous subchapter.

The computation was performed for seismotectonic model SK2011, return periods 475 and 10 000 years, minimum distance of attenuation relation 3 km and for IPEs Stromeyer and Grünthal (2009) and Labák (2000). The hazard maps are presented in Fig. 33 - Fig 36.

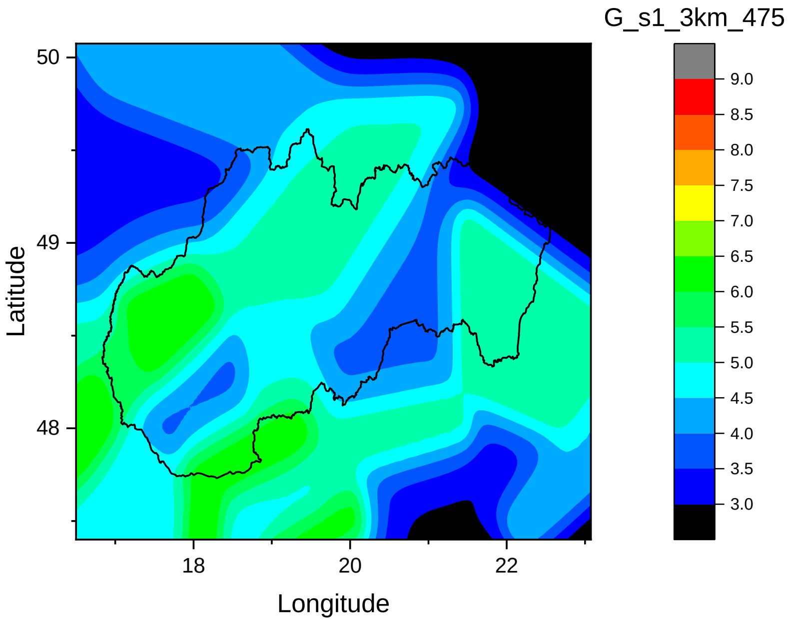

Fig. 33: Seismic hazard map computed by IPE Stromeyer and Grünthal (2009) with the minimum distance of attenuation relation 3 km, ε = 1 and for return period of 475 years.

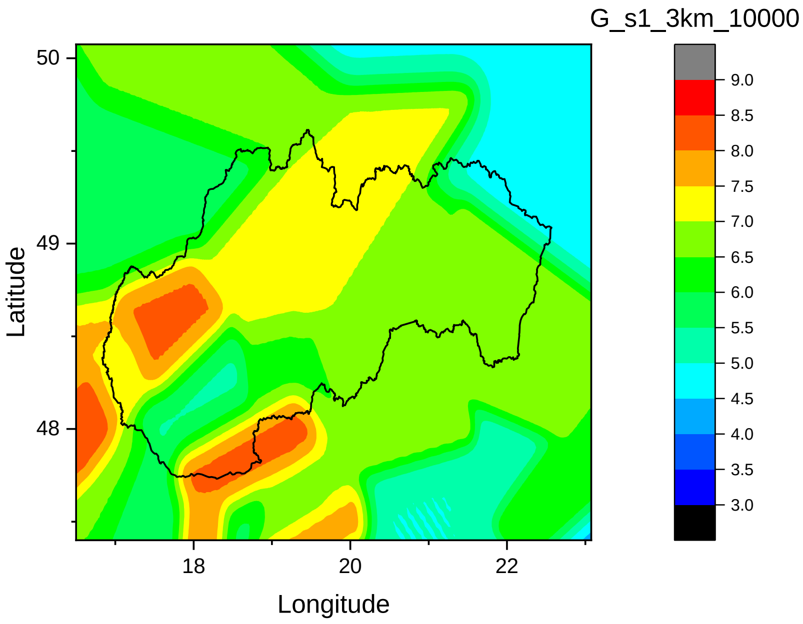

Fig. 34: Seismic hazard map computed by IPE Stromeyer and Grünthal (2009) with the minimum distance of attenuation relation 3 km, ε = 1 and for return period of 10 000 years.

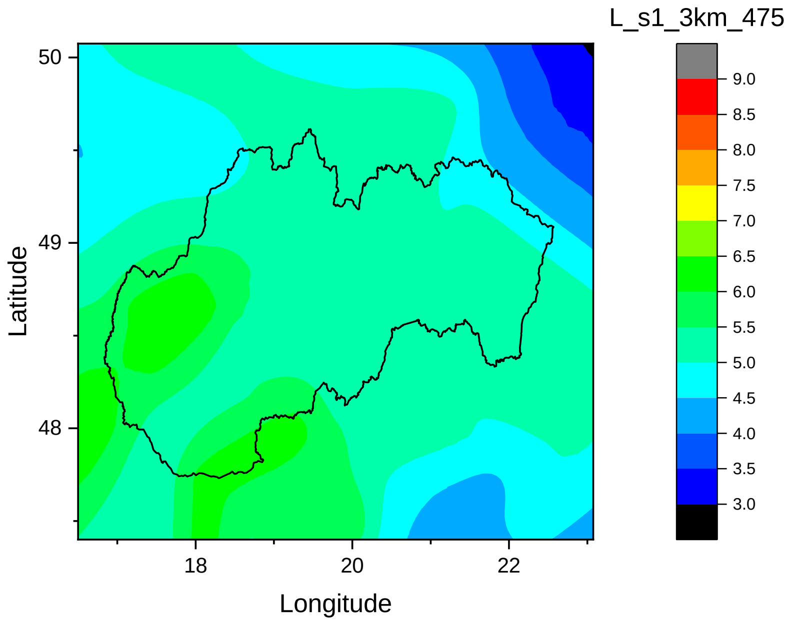

Fig. 35: Seismic hazard map computed by IPE Labák (2000) with the minimum distance of attenuation relation 3 km, ε = 1 and for return period of 475 years.

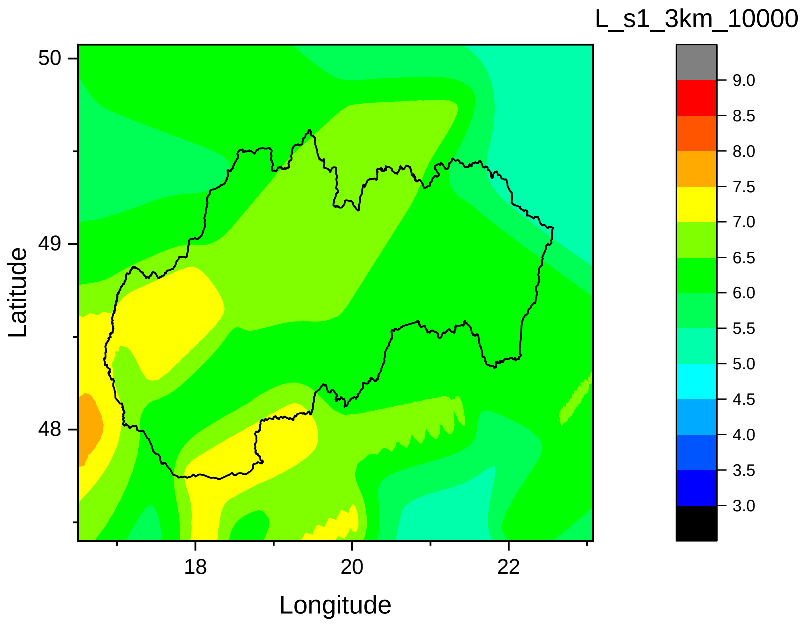

Fig. 36: Seismic hazard map computed by IPE Labák (2000) with the minimum distance of attenuation relation 3 km, ε = 1 and for return period of 10 000 years.

As we can see in Fig. 33 – Fig. 36, such truncated data for $\varepsilon = 1$ give smaller resulting values of macroseismic intensity than standardly used $\varepsilon = 3$. Moreover we can again see zig-zag structures on borders of contour plot in Fig. 36.

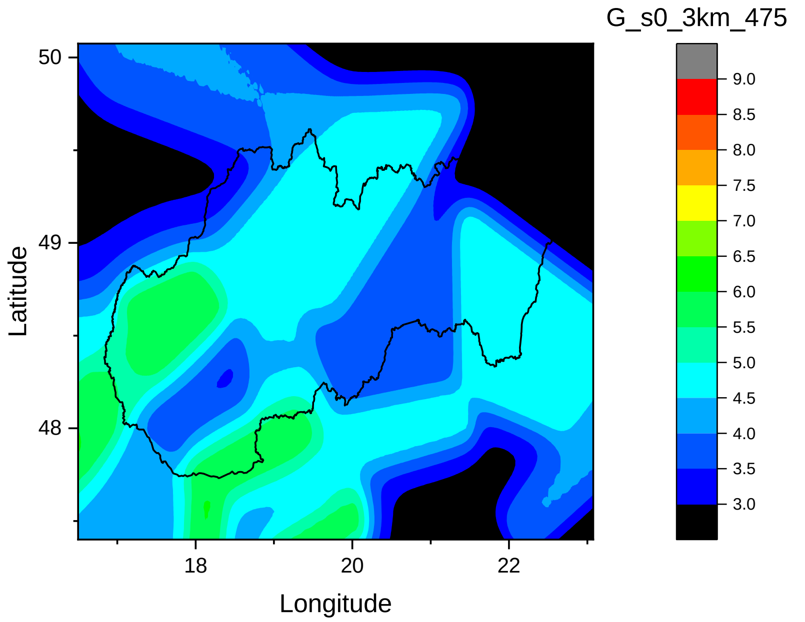

Fig. 37: Seismic hazard map computed by IPE Stromeyer and Grünthal (2009) with the minimum distance of attenuation relation 3 km, ε = 0 and for return period of 475 years.

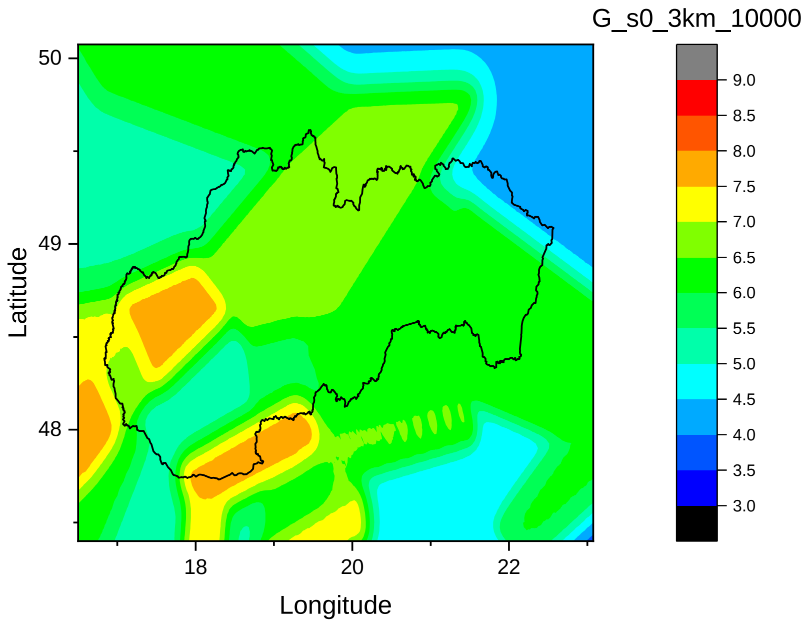

Fig. 38: Seismic hazard map computed by IPE Stromeyer and Grünthal (2009) with the minimum distance of attenuation relation 3 km, ε = 0 and for return period of 10 000 years.

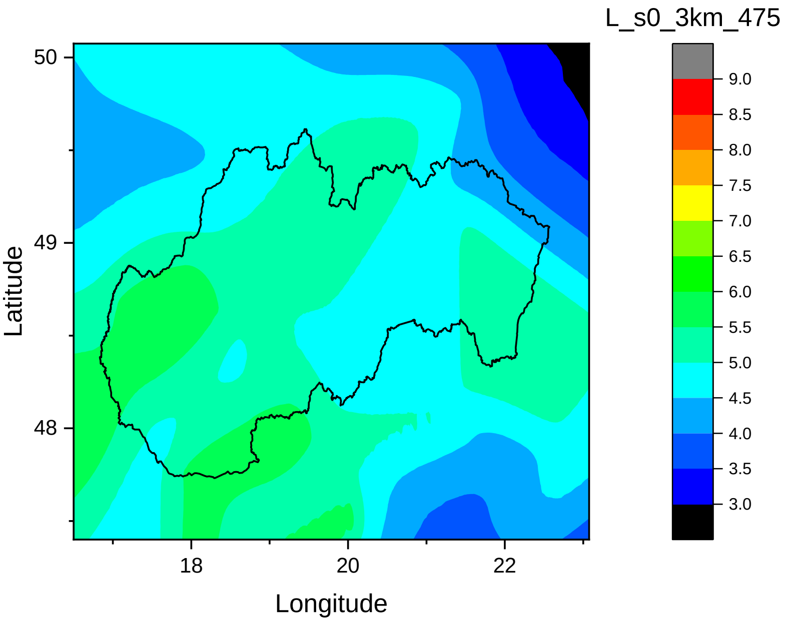

Fig. 39: Seismic hazard map computed by IPE Labák (2000) with the minimum distance of attenuation relation 3 km, $\varepsilon = 0$ and for return period of 475 years.

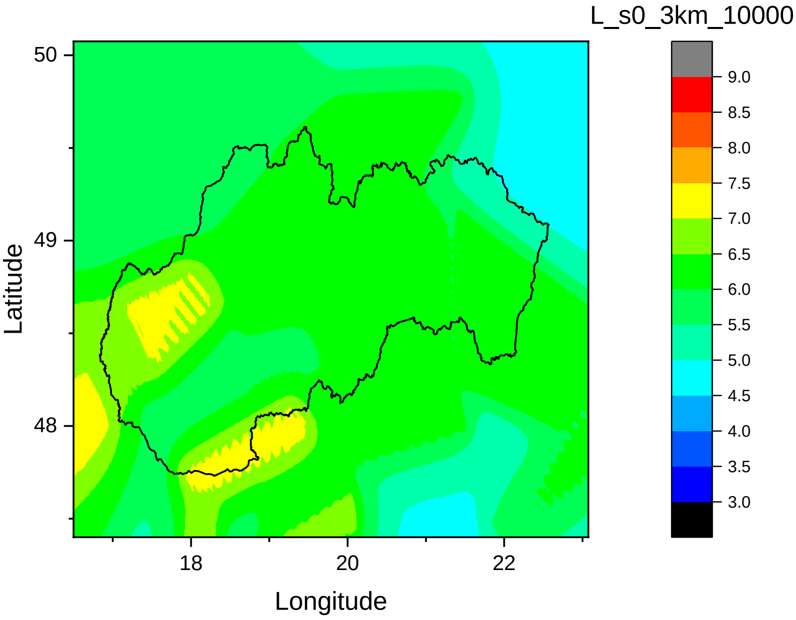

Fig. 40: Seismic hazard map computed by IPE Labák (2000) with the minimum distance of attenuation relation 3 km, $\varepsilon = 0$ and for return period of 10 000 years.

We can clearly see, that truncation $\varepsilon = 0$ gives moderately smaller values of macroseismic intensity than previous sets of input parameters. It was expected, because in such case we use only the mean values of ground motion (we neglect the variability of ground motion represented by standard deviation σ of IPE).

The effect of untruncated distribution of ground-motion residuals on the computed hazard map is shown in Fig. 41 and Fig. 42. We show only the results for IPE Stromeyer and Grünthal (2009).

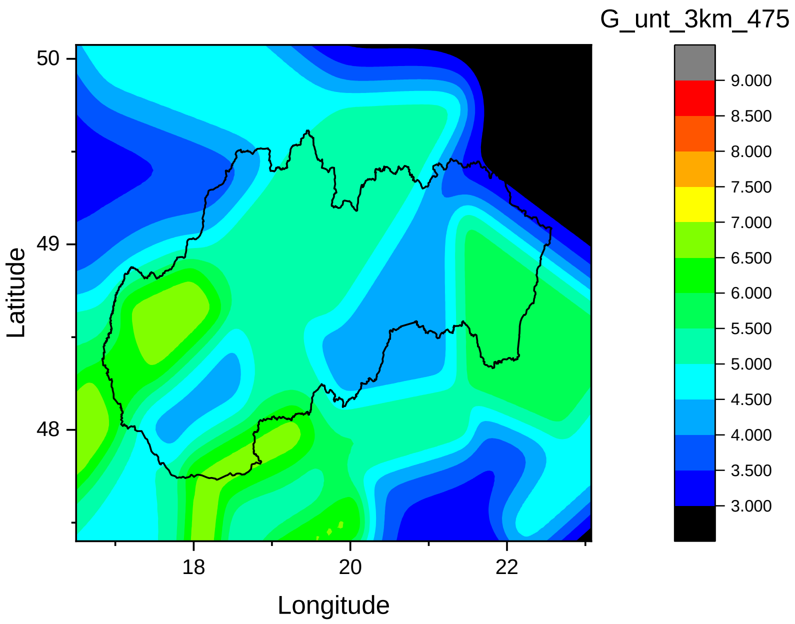

Fig. 41: Seismic hazard map computed by IPE Stromeyer and Grünthal (2009) with the minimum distance of attenuation relation 3 km, no truncation and for return period of 475 years.

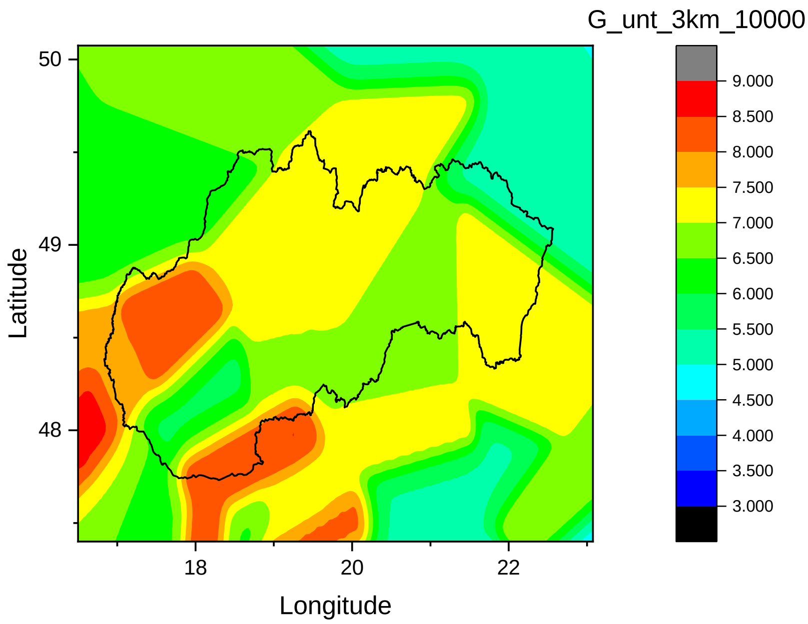

Fig. 42: Seismic hazard map computed by IPE Stromeyer and Grünthal (2009) with the minimum distance of attenuation relation 3 km, no truncation and for return period of 10 000 years.

The presented maps correspond to the well-known fact that the truncation of distribution of ground-motion residuals have significant effect on the seismic hazard for long return periods (in our case 10 000 years) and has only slight effect for return period 475 years. The seismic hazard maps for untruncated distribution show the highest values of seismic hazard and the value of $\varepsilon = 0$ give the lowest values of seismic hazard.

8.3 Effect of minimum distance of attenuation relation

To show the effect of minimum distance of attenuation relation on seismic hazard, we changed the value of the distance from 3 km to 5 km. The computation was performed for seismotectonic model SK2011, return periods 475 and 10 000 years, the truncation of distribution of ground-motion residuals $\varepsilon = 3$ and for IPEs Stromeyer and Grünthal (2009) and Labák (2000). The results are presented in Fig. 43 - Fig 46.

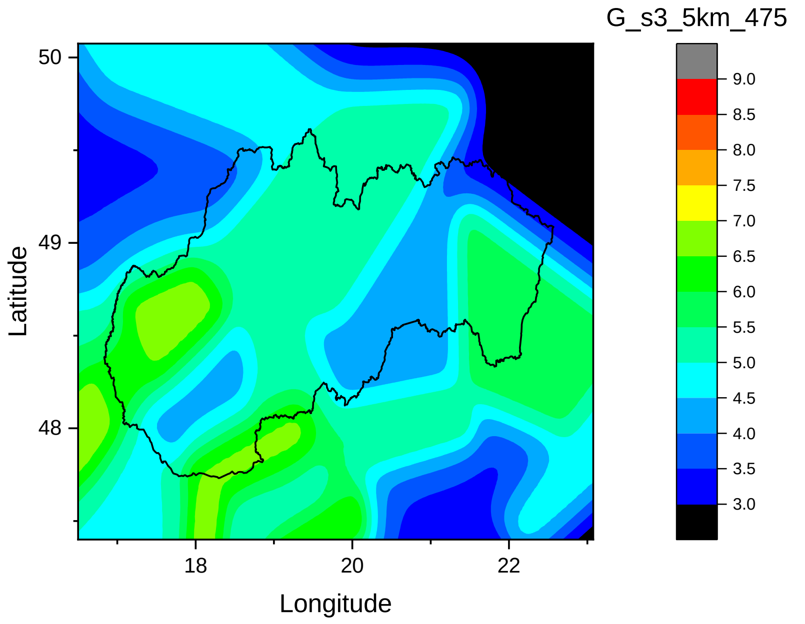

Fig. 43: Seismic hazard map computed by IPE Stromeyer and Grünthal (2009) with the minimum distance of attenuation relation 5 km, ε = 3 and for return period of 475 years.

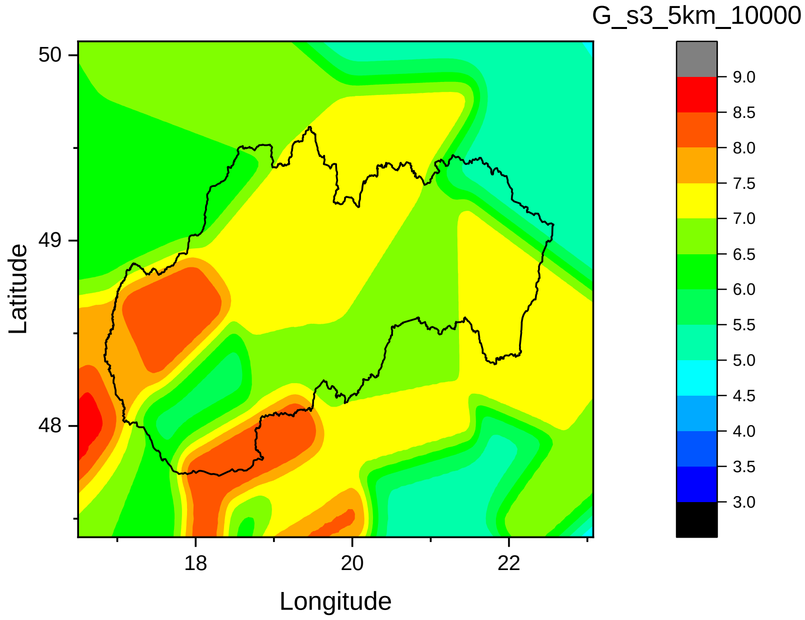

Fig. 44: Seismic hazard map computed by IPE Stromeyer and Grünthal (2009) with the minimum distance of attenuation relation 5 km, ε = 3 and for return period of 10 000 years.

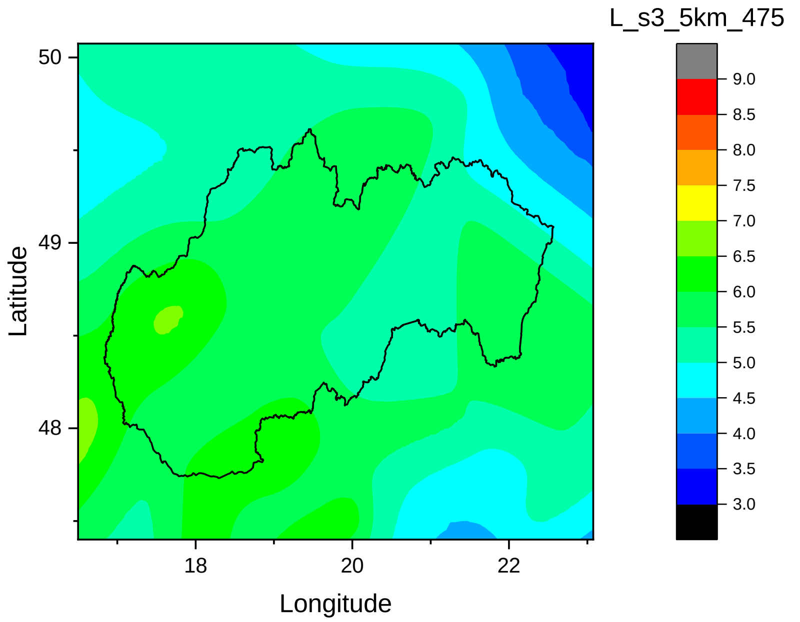

Fig. 45: Seismic hazard map computed by IPE Labák (2000) with the minimum distance of attenuation relation 5 km, ε = 3 and for return period of 475 years.

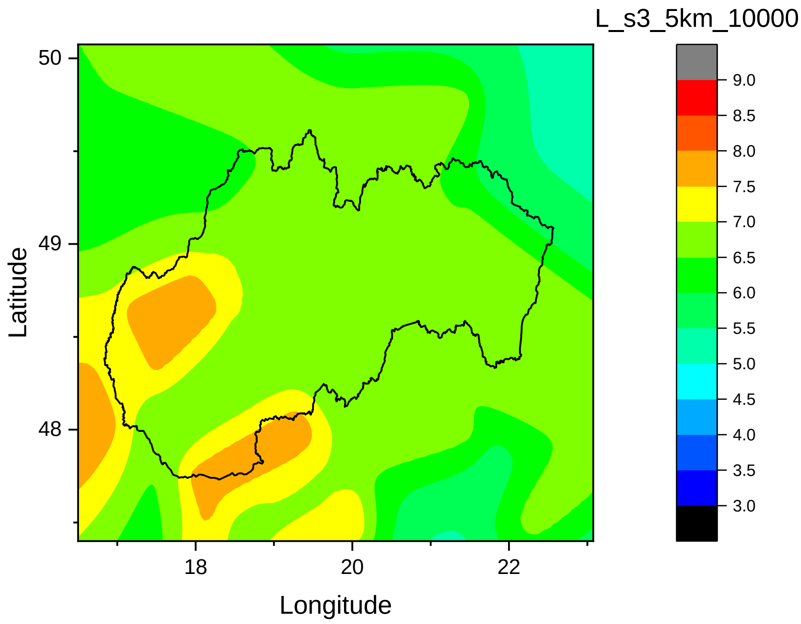

Fig. 46: Seismic hazard map computed by IPE Labák (2000) with the minimum distance of attenuation relation 5 km, ε = 3 and for return period of 10 000 years.

We can see, that this set of parameters gives results comparable with the results for the minimum distance of attenuation relation 3 km and ε = 3.

8.4 Seismic hazard maps using seismotectonic model SK2011 and IPEs depending on moment magnitude

Besides the IPEs with site intensity depending on epicentral intensity we tried to use IPEs with site intensity depending on moment magnitude: Bakun (2006), Bakun and Scotti (2006) and Pasolini et al. (2008).

The computation was performed for seismotectonic model SK2011, ε = 3, return periods 475 and 10 000 years and minimum distance of attenuation relation 3 km.

The results are presented in Fig. 47 - Fig 52.

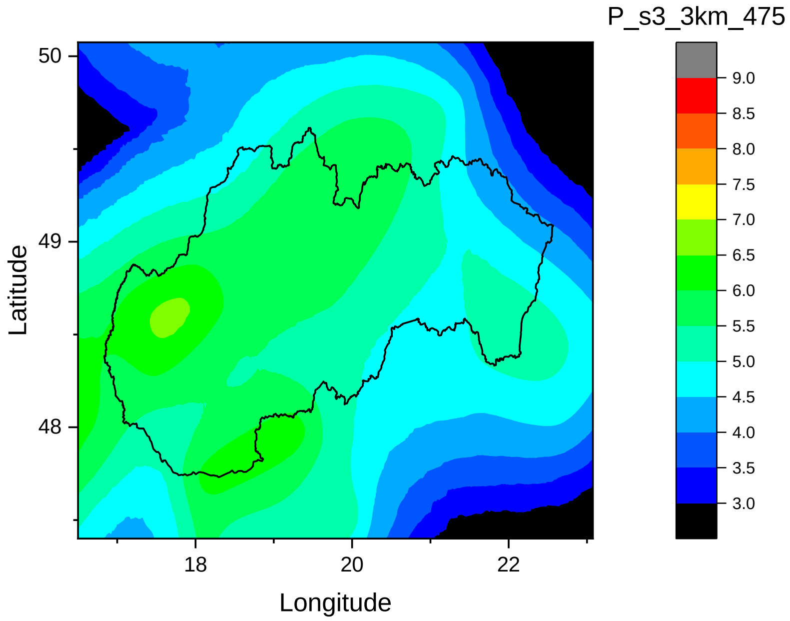

Fig. 47: Seismic hazard map computed by IPE Pasolini et al. (2008) with the minimum distance of attenuation relation 3 km, ε = 3 and for return period of 475 years.

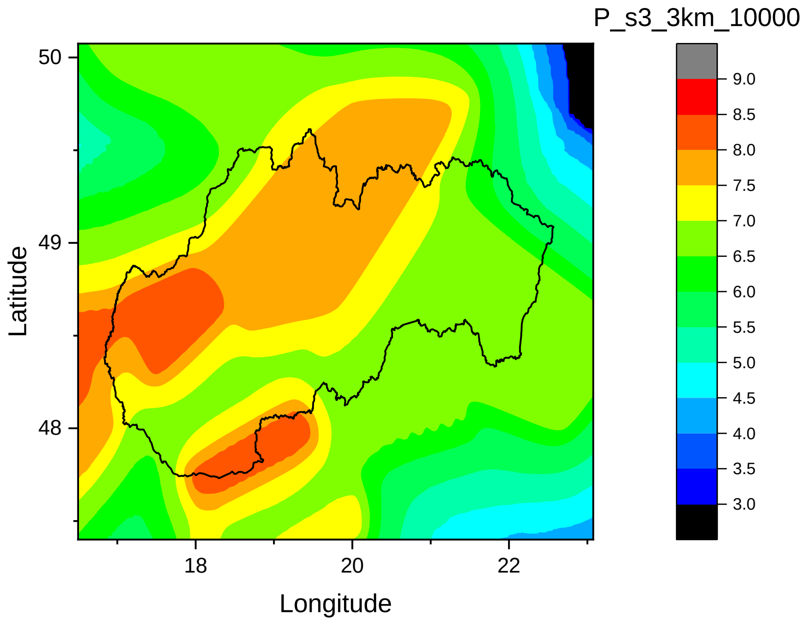

Fig. 48: Seismic hazard map computed by IPE Pasolini et al. (2008) with the minimum distance of attenuation relation 3 km, ε = 3 and for return period of 10 000 years.

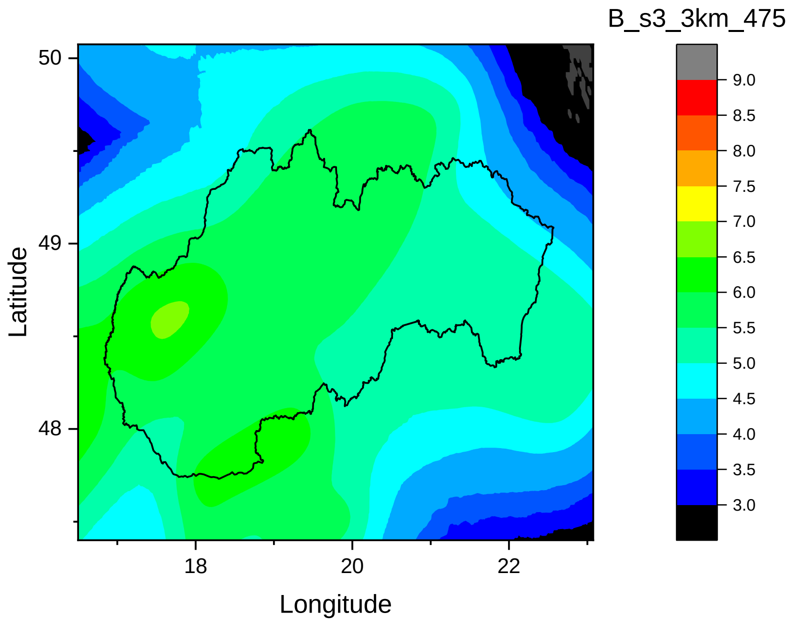

Fig. 49: Seismic hazard map computed by IPE Bakun (2006) with the minimum distance of attenuation relation 3 km, ε = 3 and for return period of 475 years.

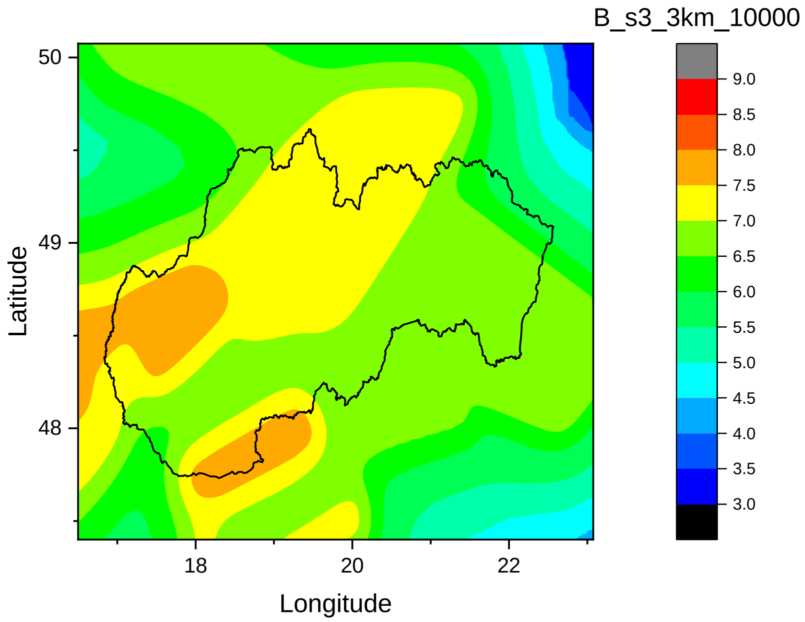

Fig. 50: Seismic hazard map computed by IPE Bakun (2006) with the minimum distance of attenuation relation 3 km, ε = 3 and for return period of 10 000 years.

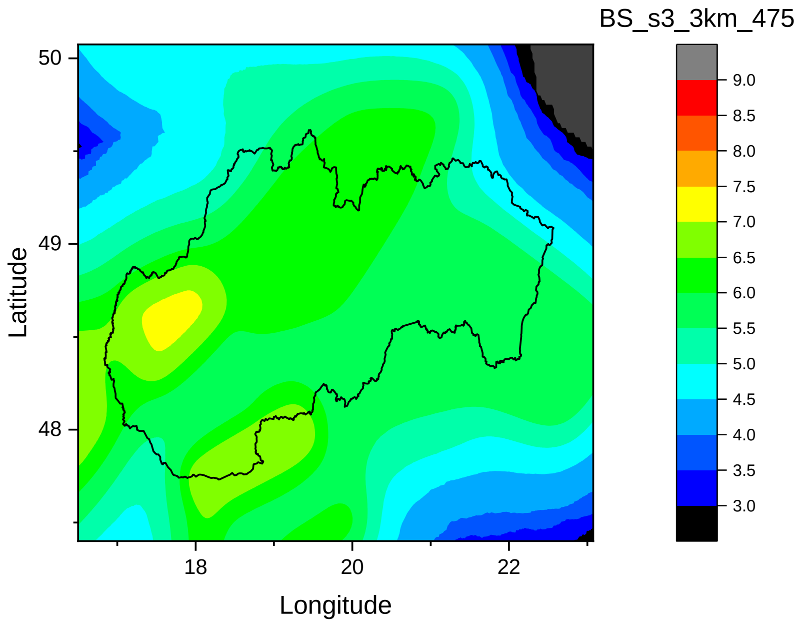

Fig. 51: Seismic hazard map computed by IPE Bakun and Scotti (2006) with the minimum distance of attenuation relation 3 km, ε = 3 and for return period of 475 years.

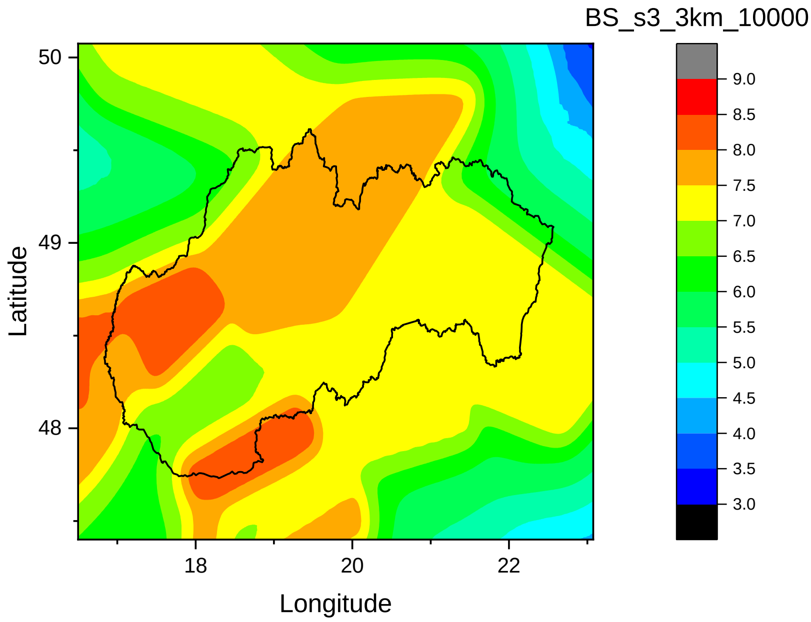

Fig. 52: Seismic hazard map computed by IPE Bakun and Scotti (2006) with the minimum distance of attenuation relation 3 km, ε = 3 and for return period of 10 000 years.

As we can see, the results vary for each IPE used, but they give results comparable with the results obtained by IPEs with site intensity depending on epicentral intensity.

8.5 Seismic hazard maps using seismotectonic model SESAME and IPEs depending on epicentral intensity

Alternatively we also tried to use seismotectonic model SESAME. The results for the minimum distance of attenuation relation 3 km, $\varepsilon = 3$, IPE Bakun (2006) and for return periods 475 and 10 000 years are presented in Fig. 53 and Fig. 54.

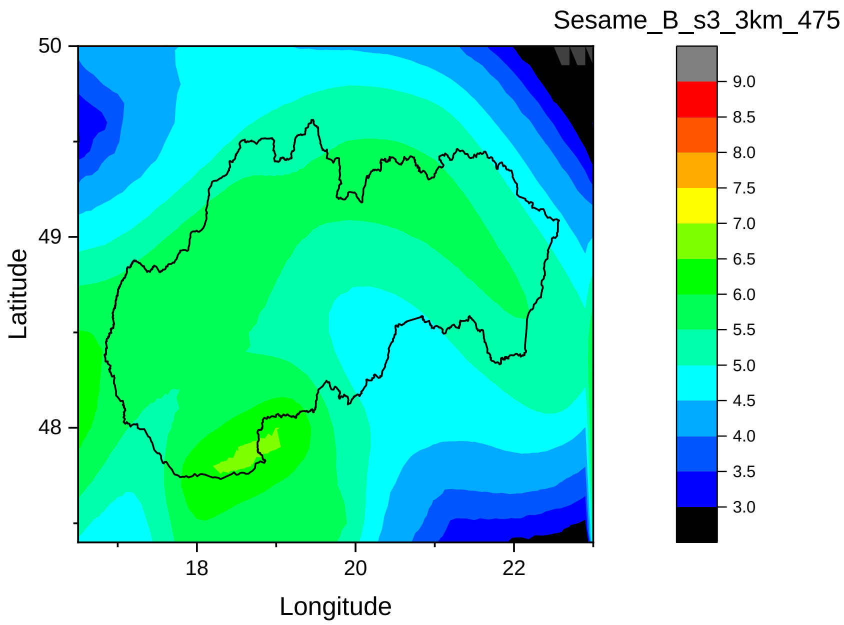

Fig. 53: Seismic hazard map computed by IPE Bakun (2006) with the minimum distance of attenuation relation 3 km, $\varepsilon = 3$ for seismotectonic model SESAME and for return period of 475 years.

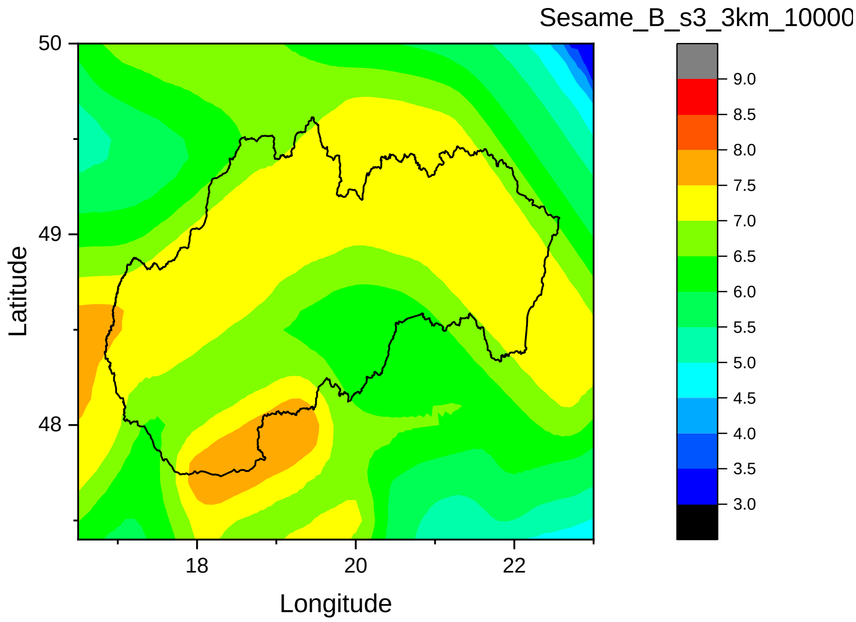

Fig. 54: Seismic hazard map computed by IPE Bakun (2006) with the minimum distance of attenuation relation 3 km, ε = 3 for seismotectonic model SESAME and for return period of 10 000 years.

As we can see, different seismotectonic model affects the shape of borders of contour plot significantly, but it does not affect the values of macroseismic intensity. The values of macroseismic intensity in Fig. 53 and Fig. 54 are in good agreement with the results for seismotectonic model SK2011.

The values of macroseismic intensity for our resulting maps are in a close agreement with the map resulting from project GSHAP (Fig. 6). However we can see a big difference in areas with the highest values of seismic hazard. The map resulting from project GSHAP shows the highest values of seismic hazard for the area near Komárno and near Žilina. That corresponds with two of the largest observed earthquakes in Slovakia – Komárno (1763) and Žilina (1858). However, the newly computed seismic hazard maps show the highest values of seismic hazard for the areas near Komárno and near Trnava. The area of Trnava corresponds to one of the largest observed earthquakes in Slovakia – 1906 Dobrá Voda earthquake (Dobrá Voda is a small village in the district of Trnava). This difference is possibly caused by different seismotectonic models and earthquake catalogues used for the computations in the GSHAP project.

8.6 Seismic hazard curves

Outcome of the seismic hazard computation is the seismic hazard curve. The curve shows graphical dependance of the annual number of exceedances of the ground motion characteristic. The inverse value of annual number of exceedances is return period. We show the seismic hazard curves for Bratislava, the capital city of Slovakia. We decided to compute seismic hazard curves for minimum distance of attenuation relation 3 km and $\varepsilon = 3$. In Fig. 55 we can see seismic hazard curves for IPEs with site intensity depending on macroseismic intensity using both seismotectonic models SK2011 and SESAME. In Fig. 56 we can see seismic hazard curves for all used IPEs with site intensity depending on moment magnitude.

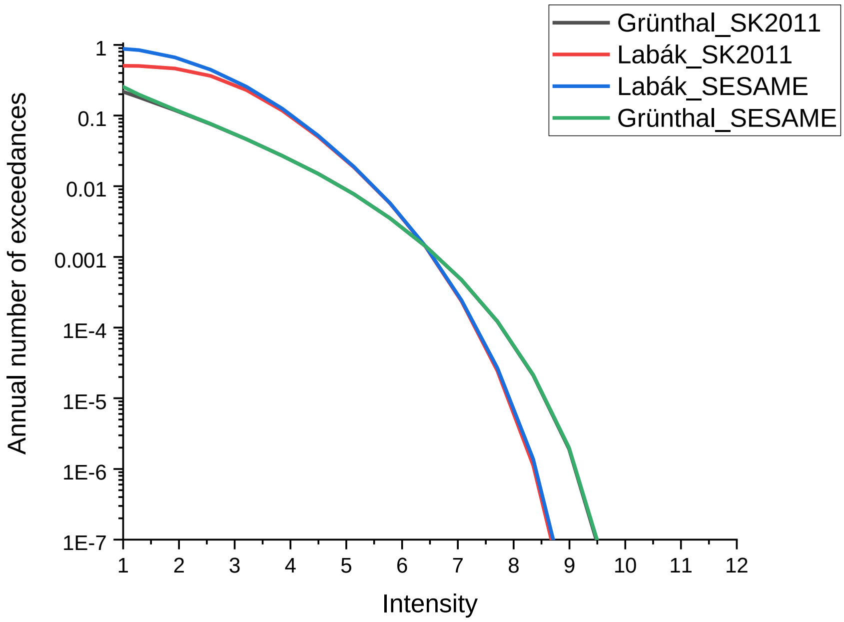

Fig. 55: Seismic hazard curves for Bratislava using ε = 3, IPEs with site intensity depending on macroseismic intensity and seismotectonic models SK2011 and SESAME.

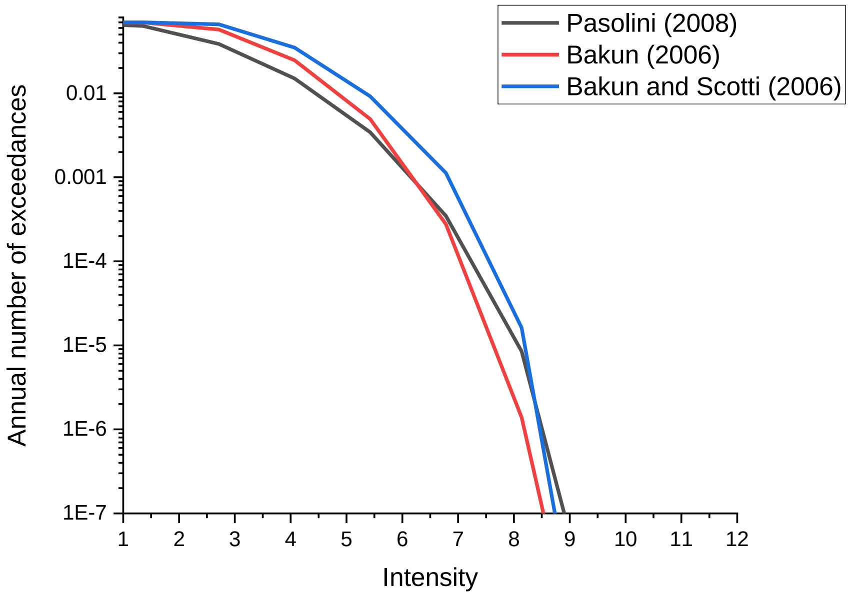

Fig. 56: Seismic hazard curves for Bratislava using ε = 3, IPEs with site intensity depending on moment magnitude and seismotectonic model SK2011.

As we can see in Fig. 55, the change of seismotectonic model did not significantly affect the values of annual number of exceedances. The annual number of exceedances for earthquakes with high intensity are nearly the same and the annual exceedances for earthquakes with low intensities are similar. In Fig. 56 we can see that the annual exceedances for all presented IPEs using site intensity depending on moment magnitude are in good agreement.

Conclusions

We computed the seismic hazard of the Slovak territory using classical approach to probabilistic seismic hazard analysis. This approach uses statistical methods and allows us to use various alternative input parameters. The probabilistic seismic hazard analysis in terms of macroseismic intensity can be described by four main steps – determination of seismic source zones, characterization of seismic source zones by input parameters, selection of IPEs and the computation of seismic hazard.

The first important step was the compilation of earthquake catalogue. The sources for the compiled catalogue were five national and two regional catalogues for the Slovak territory and neighbouring countries. We searched for duplicities and excluded them from the catalogue, leaving only one primary entry. We homogenized the earthquake catalogue so that all entries also include the moment magnitude. Using window method and cluster method we identified foreshocks, mainshocks and aftershocks. By cumulative visual method and Stepp method we determined the completeness of catalogue in time.

We used the seismotectonic model SK2011 (Hók et al., 2016), which differentiates seismic source zones based on epicentres of earthquakes and geological, tectonic and geophysical data. It is important to note that the seismic source zones of neighbouring coutries also add to the seismic hazard of Slovakia – mainly the seismic source zone of Vrancea in Romania which affects the area of eastern Slovakia. We didn´t consider this seismic source zone because the seismotectonic model SK2011 does not cover the area of Romania and also the area of Vrancea has a very different seismic regime than the area of Slovakia, therefore it would be neccessary to use different attenuation equations. The area of Vrancea is going to be investigated in future works.

We characterized the seismic source zones by the Gutenberg-Richter parameters and seismic activity rate. We determined the maximum potential intensity for every seismic source zone. The Gutenberg-Richter parameters were denoted by cumulative least squares method. The maximum potential intensity was determined as the maximum observed intensity for the seismic source zone plus half-intensity degree.

We considered available intensity prediction equations (IPEs) and we selected those, which attenuation of macroseismic intensity was comparable to the attenuation in Western Carpathians or those, which use the suitable macroseismic intensity scale. We selected five intensity prediction equations – two with site intensity depending on epicentral intensity and three with site intensity depending on moment magnitude.

We considered various alternative parameters for the computation of seismic hazard map, mainly two seimotectonic models (SESAME, SK2011), four levels of truncation of the distribution of ground-motion residuals, five intensity prediction equations. We discussed the changes of the results caused by the changes of the input parameters.

The computations were executed for the grid of 28 512 points covering the area of Slovakia and small parts of neighbouring countries. For each computational point, the seismic hazard curve was computed and the macroseismic intensity for return periods of 475 years (10% probability of exceedance in 50 years) and 10 000 years (which should match the intensities of highest observed earthquakes in every seismic source zone) was determined.

The results are in close agreement with previous seismic hazard analysis of the Slovak territory (results from the GSHAP project). The biggest difference is in the location of the areas with highest values of seismic hazard – previous analysis shows the highest values near Žilina and our computations near Trnava. This is probably caused by different seismotectonic models and earthquake catalogues.

Truncation of the distribution of ground-motion residuals has strong impact on the results. The frequently used value of truncation $\varepsilon = 3$ results in macroseismic intensity values similar to the previous seismic hazard analysis. The largest values of seismic hazard were given by untruncated distribution of ground-motion residuals. This effect is significant for return period of 475 years and negligible for return period of 10 000 years. This is well known fact and our results are in a good agreement with it.

In cases of epistemic uncertainty of input parameters we standardly use the logic-tree approach. The presented results will be analyzed using the logic-tree approach with the goal to develop a final seismic hazard map. We proposed that the nodes of logic-tree need to be seismotectonic model and IPEs. We showed that declustering and time completeness do not need to be considered in the logic-tree. The further investigation of depth of seismic source zones and uncertainty in Gutenberg-Richter parameters will be our future work.

References

ACORN, 2004. Catalogue of Earthquakes in the Region of the Alps – Western Carpathians - Bohemian Massif for the period from 1267 to 2004, Computer File. Vienna (Central Institute for Meteorology and Geodynamics, Department of Geophysics) - Brno (Institute of Physics of the Earth, University Brno).

Atkinson, G. M., Wald, D. J., 2007. "Did You Feel It?" intensity data: A surprisingly good measure of earthquake ground motion. *Seismological Research Letters* 78, 362-368.

Bakun, W. H., Johnston, A. C., Hopper, M. G., 2003. Estimating locations and magnitudes of earthquakes in eastern North America from Modified Mercalli Intensities. *Bulletin of the Seismological Society of America* 93, 190-202.

Bakun, W. H., Scotti, O., 2006. Regional intensity attenuation models for France and the estimation of magnitude and location of historical earthquakes. *Geophysical Journal International* 164, 596–610.

Bakun, W. H., Wentworth, C. M., 1997. Estimating earthquake location and magnitude from seismic intensity data. *Bulletin of the Seismological Society of America* 87, 1502-1521.

Bolt, B. A., Miller, R. D., 1969. Seismicity of northern and central California. 1965-1969. *Bulletin of the Seismological Society of America* 61, 1831-1847.

Burkhard, M., Grünthal, G., 2009. Seismic source zone characterization for the seismic hazard assessment project PEGASOS by the Expert Group 2 (EG 1b). *Swiss Journal of Geosciences* 102, 149-188.

Cua, G., Wald D. J., Allen, I. T., Garcia, D., Worden, B. C., Gerstenberger, M., Lin, K., Marano, K., 2010. „Best Practices" for Using Macroseismic Intensity and Ground Motion-Intensity Conversion Equations for Hazard and Loss Models in GEM1. *GEM Technical Report 2010-4*, GEM Foundation, Pavia, Italy.

Decker, K., Gangl, G., Kandler, M., 2006. The earthquake of Carnuntum in the fourth century A.D. – archeological results, seismologic scenario and seismotectonic implications for the Vienna Basin fault, Austria. *Journal of Seismology* 10, 479-495.

Douglas, J., 2016. Ground motion prediction equations 1964-2016. Available online: *http://www.gmpe.org.uk/gmpereport2014.pdf.*

GPI CAS, 2012. Katalog regionálních seismických jevů zaznamenané českou regionální seismologickou sítí. Data file. Geophysical institute of Czech Academy of Sciences, Prague.

GPI SAS, 2011. Katalóg zemetrasení lokalizovaných na území Slovenska (Version 2009). Geophysical institute of Slovak Academy of Sciences, Bratislava. Data file.

Grünthal, G., 1998. European Macroseismic Scale 1998 (EMS-98). European Seismological Commission, sub commission on Engineering Seismology, Working Group Macroseismic Scales. Conseil de l'Europe, Cahiers du Centre Européen de Géodynamique et de Séismologie, Vol. 15, Luxembourg.

Grünthal, G., Wahlström, R., 2012. The European-Mediterranean Earthquake Catalogue (EMEC) for the last millenium. *Journal of Seismology* 16, 535-570.

Grünthal, G., Wahlström, Stromeyer, D., 2009. The unified catalogue of earthquakes in central, northern, and northwestern Europe (CENEC) – updated and expanded to the last millenium. *Journal of Seismology* 13, 517-541.

Gutenberg, R., Richter, C. F., 1944. Frequency of earthquakes in California. *Bulletin of the Seismological Society of America* 34, 185-188.

Kramer, S., 1996. *Geotechnical Earthquake Engineering*. Prentice Hall, Upper Saddle River, New Jersey.

Kysel, R., 2014. Seizmické ohrozenie územia Slovenska. Rigorous Thesis [in Slovak]. Faculty of Mathematics, Physics and Informatics, Comenius University in Bratislava. 106 pgs.

Labák, P., 2000. Pravdepodobnostný výpočet charakteristík seizmického ohrozenia pre lokalitu atómových elektrární Bohunice. PhD. Thesis [in Slovak]. Faculty of Mathematics, Physics and Informatics, Comenius University in Bratislava. 121 pgs.

McGuire, R., 2008. Probabilistic seismic hazard analysis: Early history. *Earthquake Engineering and Structural Dynamics* 37, 329-338.

Molchan, G., Dmitrieva, O., 1992. Aftershock identification: methods and new approaches, *Geophysical Journal International*, 109, 501-516.

Musson, R. M. W., Grünthal, G., Stucchi, M., 2009. The comparison of macroseismic intensity scales. *Journal of Seismology*. 14 (2), 413-428.

Pasolini C., Albarello D., Gasperini P., D'Amico V and Lolli B., 2008. The attenuation of seismic intensity in Italy, part II: modeling and validation. *Bulletin of the Seismological Society of America* 98, 692-708.

Reasenberg, P., 1985. Second-order moment of central California seismicity. 1969-82, *Journal of Geophysical Research* 90, 5479-5495.

Reiter, L., 1990. *Earthquake Hazard Analysis. Issues and Insights.* Columbia University Press, New York.

Jiménez, M.-J., Giardini, D., Grünthal, G., 2003. The ESC-SESAME unified hazard model for the European-Mediterranean region. *EMSC/CSEM Newsletter* 19, 2-4.

Schenk, V., Schenková, Z., Kottnauer, P., Guterch, B., Labák, P., 2000. Earthquake hazard for the Czech Republic, Poland and Slovakia - contribution to the ILC/IASPEI Global seismic hazard assessment program. *Natural Hazards* 21, 331-345.

Stepp, J. C., 1972. Analysis of completeness of the earthquake sample in the Puget Sound area and its effect on statistical estimates of earthquake hazard. In: *Proceedings of the International Conference on Microzonation*, vol. 2, 897-910.

Šugár, M., 2016. Analýza seizmického ohrozenia územia Slovenska v hodnotách makroseizmickej intenzity. Bachelor Thesis [in Slovak]. Faculty of Mathematics, Physics and Informatics of Comenius University in Bratislava. 55 pgs.

Trifunac, M. D., Brady, A. G., 1975. On the correlation of seismic intensity scales with the peaks of recorded strong ground motion. *Bulletin of Seismological Society of America* 65, 139-162.

Uhrhammer, R., 1986. Characteristics of Northern and Central California Seismicity. Earthquake Notes, 57, 21.

Wiemer, S., M. García-Fernández, J.-P. Burg, 2009. Development of a seismic source model for probabilistic seismic hazard assessment of nuclear power plant sites in Switzerland: the view from PEGASOS Expert Group 4 (EG1d). *Swiss Journal of Geosciences* 102, 189-209.

ZAMG 2011. Catalogue of regional seismic events-Austrian Regional Seismological Network. Computer file. Zentralanstalt für Meteorologie und Geodynamik, Vienna.

Zsíros, T., Mónus, P., Tóth, L., 1988. Hungarian earthquake catalogue (456-1986). Geodetic and Geophysical Research Institute, Hungarian Academy of Sciences, Budapest.

Abstract

Martin Šugár: *Seismic hazard of the Slovak territory characterized by the macroseismic intensity.* [Master´s thesis]. Comenius University in Bratislava. Faculty of Mathematics, Physics and Informatics, Department of Astronomy, Physics of the Earth and Meteorology. Supervisor: RNDr. Róbert Kysel, PhD. Bratislava 2018. 90 pgs. Degree of qualification: Master.

In the Master´s thesis we deal with the probabilistic seismic hazard analysis of the territory of Slovakia. We used the classical Cornell-McGuire approach to probabilistic seismic hazard analysis. We compiled the earthquake catalogue from available catalogues for the territory of Slovakia and neighbouring countries and we analyzed it. The result of the Master´s Thesis is the set of seismic hazard maps for the territory of Slovakia, which analyzes the effects of input parameters on seismic hazard. We compared the obtained results with the results of previous seismic hazard analyses of the territory of Slovakia.

Abstrakt

Martin Šugár: Seismische Gefährdung des slowakischen Gebiets durch makroseismische Intensität. [Master-Arbeit]. Comenius-Universität in Bratislava. Fakultät für Mathematik, Physik und Informatik, Abteilung für Astronomie, Physik der Erde und Meteorologie. Betreuer: RNDr. Róbert Kysel, PhD. Bratislava 2018. 90 Stn. Qualifikationsgrad: Master.

Die Masterarbeit beschäftigt sich mit der probabilistischen Analyse der seismischen Gefährdung des slowakischen Territoriums. Dazu wird der klassische Cornell-McGuire-Ansatz verwendet. Im Rahmen der Masterarbeit wurde ein Erdbebenkatalog aus verfügbaren Daten für das Gebiet der Slowakei und der Nachbarländer zusammengestellt und analysiert. Als Ergebnis liegt ein Satz seismischer Gefährdungskarten für das Gebiet der Slowakei vor, mit dem die Auswirkung der Inputparameter auf die seismische Gefährdung analysiert wird. Die Resultate werden mit denen früherer seismischer Gefährdungsanalysen des slowakischen Territoriums verglichen.

CURRICULUM VITAE

Personal information

Date of birth:	18.02.1994
Address:	Koniarekova 4, 91701 Trnava
Mobile:	+421 910 146 986
E-mail:	martin.sugar@savba.sk

Education

2016 -	Comenius University in Bratislava Faculty of Mathematics, Physics and Informatics University of Vienna Branch of study: Joint Master Study Programme Physics of the Earth, degree: MSc.
2012 - 2016	Comenius University in Bratislava Faculty of Mathematics, Physics and Informatics Branch of study: Physics , degree: Bc.